AD

ANALYSIS AND EVALUATION OF SUPPRESSIVE SHIELDS

by

P. A. Cox
P. S. Westine
J. J. Kulesz
E. D. Esparza

January 1978

SOUTHWEST RESEARCH INSTITUTE
Post Office Drawer 28510, 6220 Culebra Road
San Antonio, Texas 78284

D D C

RECEIVED
MAR 21 1978
D

DEPARTMENT OF THE ARMY
Headquarters, Edgewood Arsenal
Aberdeen Proving Ground, Maryland 21010

ADA051583

AU No.
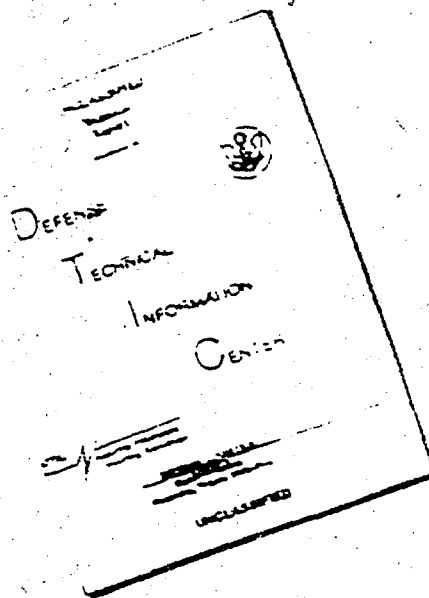DDC FILE COPY

DISCLAIMER NOTICE

THIS DOCUMENT IS BEST QUALITY AVAILABLE. THE COPY FURNISHED TO DTIC CONTAINED A SIGNIFICANT NUMBER OF PAGES WHICH DO NOT REPRODUCE LEGIBLY.

SWRI-02-4164

REPORT DOCUMENTATION PAGE

READ INSTRUCTIONS
BEFORE COMPLETING FORM

1. REPORT NUMBER	2. GOVT ACCESSION NO.	3. RECIPIENT'S CATALOG NUMBER
ARCSL CR-77028		Report No. 10 (Final) Jun 76 - Jun 77

4. TITLE (and Subtitle)	5. TYPE OF REPORT & PERIOD COVERED
ANALYSIS AND EVALUATION OF SUPPRESSIVE SHIELDS	Final Technical Report, June 1976 - June 1977
	6. PERFORMING ORG. REPORT NUMBER
	Report No. 10, 02-4164

7. AUTHOR(s)	8. CONTRACT OR GRANT NUMBER(s)
P. A. Cox, P. S. Westine, J. J. Kulesz, and E. D. Esparza	DAAA15-75-C-0083

9. PERFORMING ORGANIZATION NAME AND ADDRESS	10. PROGRAM ELEMENT, PROJECT, TASK AREA & WORK UNIT NUMBERS
Southwest Research Institute P.O. Drawer 28510 San Antonio, Texas 78284	PA, A 3751264

11. CONTROLLING OFFICE NAME AND ADDRESS	12. REPORT DATE
Commander, Edgewood Arsenal Attn: SAREA-TS-R Aberdeen Proving Ground, Maryland 21010	June 77
	13. NUMBER OF PAGES
	95

14. MONITORING AGENCY NAME & ADDRESS(If different from Controlling Office)	15. SECURITY CLASS. (of this report)
Commander, Edgewood Arsenal (CPO Mr. Bruce W. Jezek, 671-2661) Attn: SAREA-MT-H Aberdeen Proving Ground, Maryland 21010	UNCLASSIFIED
	15a. DECLASSIFICATION/DOWNGRADING SCHEDULE N/A

16. DISTRIBUTION STATEMENT (of this Report)

Approved for public release; distribution unlimited.

17. DISTRIBUTION STATEMENT (of the abstract entered in Block 20, if different from Report)

18. SUPPLEMENTARY NOTES

19. KEY WORDS (Continue on reverse side if necessary and identify by block number)

Suppressive shielding	Test data
Structural response	Propellant burning
Energy methods	Vented enclosures
Elastic-plastic	Pressure history
Strain rate	

20. ABSTRACT (Continue on reverse side if necessary and identify by block number)

This report documents work performed for the Edgewood Arsenal Suppressive Structures program from January 1976 through June 1977. Included in this work were the development of approximate energy solutions for the response of structures to blast loading, the analysis of strain data from the Category I 1/4-scale model tests, and calculations of pressure-time histories for the burning of M10 propellants in the Category V shield.

DD FORM 1473 EDITION OF 1 NOV 65 IS OBSOLETE
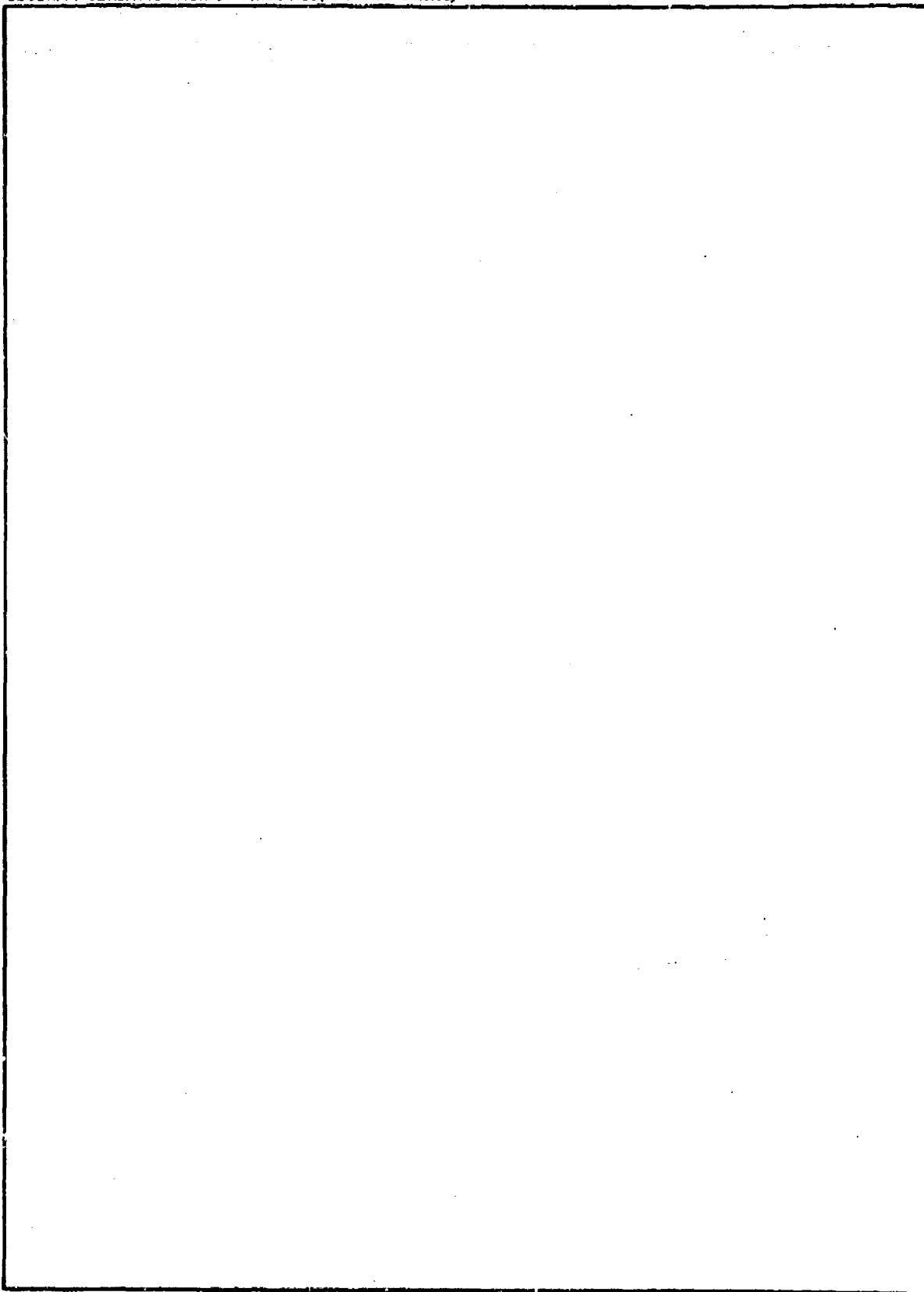
SUMMARY

This report documents work performed for the Edgewood Arsenal Suppressive Structures program from January 1976 through June 1977. Included in this work was the development of approximate energy solutions for the response of structures to blast loading, the analysis of strain data from the Category I 1/4-scale model tests, and calculation of pressure-time histories for the burning of M10 propellants in the Category V shield.

DDC

MAR 21 1978

D

3

TABLE OF CONTENTS

TABLE OF CONTENTS (Cont'd)

LIST OF ILLUSTRATIONS

LIST OF TABLES

ANALYSIS AND EVALUATION OF SUPPRESSIVE SHIELDS

I. INTRODUCTION

This final technical report documents work performed under Contract DAAA15-75-C-0083 for Edgewood Arsenal in support of the suppressive structures program. Principally, it includes work performed during the time period of January 1976 through June 1977; however, some earlier work has been included in summary form. Also, some work performed during this time period and documented in separate letter reports has not been included. Work performed prior to January 1976 is documented in References 1 through 9.

Contents of this report cover three different aspects of the work:

- The use of energy methods to predict deformations in blast-loaded structures,

- Strain data analysis for the Category I 1/4-scale model tests, and

- Calculation of pressure-time histories produced by burning propellant in vented enclosures.

Chapter II contains recent work on the development of energy solutions for structural response. This recent work includes a study of the influence of the deformed shape on the accuracy of the solution obtained, energy solutions for coupled response, energy solutions for combined elastic-plastic behavior of beams and strings and the construction of general graphical solutions for blast-loaded beams. Chapter III contains a summary of solutions which have been developed over the total contract period.

Analysis of strain data from the Category I 1/4-scale model tests is covered in Chapter IV. Comparisons are made between measured strains and strains predicted by the approximate energy methods and by finite-element methods. Chapter V describes the calculation procedures and gives results for M10 propellant burning in vented enclosures.

II. ADDITIONAL SOLUTIONS WITH ENERGY METHODS

A. Importance of the Assumed Deformed Shape

In using energy solutions to compute maximum deformations or strains in blast loaded structural components, we select a deformed shape with appropriate boundary conditions. Usually, this assumed deformed shape is either the first mode from an infinite series of modes, or the static deformed shape carried over to a dynamic analysis. We will demonstrate that either assumption can give excellent predictions of strains or deflections using *either* assumed deformed shape. This generalization pertains for both elastic and plastic response of structural components, and is true for both quasi-static and impulsive transient loads.
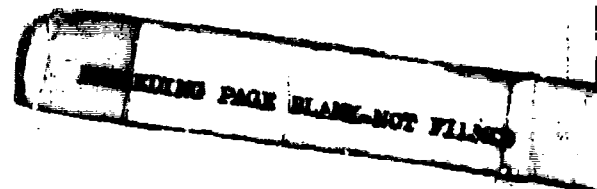
1. Influence of Higher Modes

A general deformed shape for a simply-supported elastic beam loaded with a uniform quasi-static pulse is given by Eq. (1).

$$y = w_o \sum_{N=1,3,5}^{\infty} A_N \sin \frac{N\pi x}{\ell} \qquad (1)$$

The even modes are missing because of symmetry, and cosine contributions are missing because of simply-supported boundary conditions. For bending only, the strain in the beam is

$$\epsilon = -h\frac{d^2 y}{dx^2} = \frac{\pi^2 w_o h}{\ell^2} \sum_{N=1,3,5}^{\infty} N^2 A_N \sin \frac{N\pi x}{\ell} \qquad (2)$$

In a rectangular beam, t⁓ ⁓e is given by:

$$\text{Vol.} = 4b \int_{0}^{H/2} dh \int_{0}^{\ell/2} dx \qquad (3)$$

The strain energy U is:

$$U = \int_{V} \frac{E}{2} \epsilon^2 \, dV, \qquad (4a)$$

or:

$$U = \frac{2\pi^4 E w_o^2 b}{\ell^4} \int_{0}^{H/2} h^2 \, dh \sum_{N=1,3,5}^{\infty} N^4 A_N^2 \int_{0}^{\ell/2} \sin^2\left(\frac{N\pi x}{\ell}\right) dx \qquad (4b)$$

The cross-products associated with squaring the strain integrate to zero in the preceding equation because of orthogonality of the mode shapes. Performing the required double integration gives for the strain energy:

$$U = \frac{\pi^4 E w_o^2 b H^3}{48 \, \ell^3} \sum_{N=1,3,5}^{\infty} N^4 A_N^2 \qquad (5)$$

Next we compute the maximum possible work imparted to the structure with the deformed shape of Eq. (1). This work equals:

$$wk = 2pbw_o \sum_{N=1,3,5}^{\infty} A_N \int_0^{\ell/2} \sin \frac{N\pi x}{\ell} \, dx \tag{6}$$

Or, after integrating:

$$wk = \frac{2pbw_o \ell}{\pi} \sum_{N=1,3,5}^{\infty} \frac{A_N}{N} \tag{7}$$

The Rayleigh-Ritz method can be used to obtain the relative amplitudes of the different modes. This is accomplished by subtracting the work from the strain energy,

$$(U - wk) = \frac{\pi^4 E w_o^2 bH^3}{48 \ell^3} \sum_{N=1,3,5}^{\infty} N^4 A_N^2 - \frac{2pbw_o \ell}{\pi} \sum_{N=1,3,5}^{\infty} \frac{A_N}{N} \tag{8}$$

and differentiating with respect to A_N so the energy difference is minimized. This procedure yields:

$$\frac{\partial(U - wk)}{\partial A_N} = \frac{\pi^4 E w_o^2 bH^3}{24 \ell^3} N^4 A_N - \frac{2pbw_o \ell}{\pi} \frac{1}{N} = 0 \tag{9}$$

or:

$$A_N = \left(\frac{48 p \ell^4}{\pi^5 E w_o H^3} \right) \frac{1}{N^5} \tag{10}$$

If one substitutes A_N from Eq. (10) back into the preceding equations, a series solution for the deformed shape is obtained. The influence of higher modes can be obtained by dividing A_N by the amplitude of the first mode. This step yields

$$\frac{A_N}{A_1} = \frac{1}{N^5} \tag{11}$$

For a three-mode solution, the deformed shape will equal:

$$y = mw_o \left[\sin \frac{\pi x}{\ell} + \frac{1}{243} \sin \frac{3\pi x}{\ell} + \frac{1}{3125} \sin \frac{5\pi x}{\ell} \right] \tag{12}$$

The parameter m equals 1.0038 if y is to equal w_o at mid-span (at x/ℓ to 0.5). Substituting for m, differentiating Eq. (12) twice, and multiplying by $-h$ gives the strain.

$$\epsilon = -\frac{\pi^2 w_o h}{\ell^2} (1.0038) \left[\sin \frac{\pi x}{\ell} + \frac{1}{27} \sin \frac{3\pi x}{\ell} + \frac{1}{125} \sin \frac{5\pi x}{\ell} \right] \tag{13}$$

13

From Eq. (4a),

$$U = 1.0076 \left(\frac{2\pi^4 Ebw_o^2}{\ell^4}\right) \int_0^{H/2} h^2 \, dh \int_0^{\ell/2} \left[\sin\frac{\pi x}{\ell} + \frac{1}{27}\sin\frac{3\pi x}{\ell} + \frac{1}{125}\sin\frac{5\pi x}{\ell}\right]^2 dx \quad (14)$$

Performing the double integration gives for the strain energy:

$$U = 1.053 \left(\frac{\pi^4 Ebw_o^2 H^3}{48\,\ell^3}\right) \quad (15)$$

The factor 1.053 has been separated from the other terms in the preceding equation, as this 5.3 percent increase in the strain energy U is the effect of adding the third and fifth mode contributions to the first mode estimate. A similar procedure will be followed in presenting the influence of high modes in subsequent relationships.

The work which must be equated to this strain energy is given by:

$$wk = 2pb(1.0038w_o) \int_0^{\ell/2} \left[\sin\frac{\pi x}{\ell} + \frac{1}{243}\sin\frac{3\pi x}{\ell} + \frac{1}{3125}\sin\frac{5\pi x}{\ell}\right] dx \quad (16)$$

or, after integrating:

$$wk = 1.00524 \left[\frac{2pbw_o\ell}{\pi}\right] \quad (17)$$

The influence of higher modes on the work is less than a 1 percent increase. Equating the work to the strain energy and solving for a nondimensionalized mid-span deformation, $w_o H/\ell^2$, yields:

$$\frac{w_o H}{\ell^2} = 0.9546 \left[\frac{96p\ell^2}{\pi^5 EH^2}\right] \quad (18)$$

This equation implies that the actual deformation will be less than that estimated with the one mode approximation, but the difference is less than 5 percent. The maximum strains can also be estimated. Substituting $H/2$ for h, Eq. (18) into Eq. (13), and $\ell/2$ for x gives for the maximum strain:

$$\epsilon_{max} = 0.9304 \left[\frac{48p\ell^2}{\pi^3 EH^2}\right] \quad (19)$$

Equation (19) shows that the one mode approximation also overestimates the strain in this illustration, but that this error is less than 7 percent.

14

We present one more illustration to show that these same conclusions can be reached for plastic as well as elastic response, and for extensional as well as bending behavior. As the second illustration, consider a string* with the deformed shape given by Eq. (1). The string has a different shape from a beam; however, this difference is reflected in the A_N coefficients. In a string,

$$\epsilon = \frac{1}{2}\left(\frac{dy}{dx}\right)^2 \tag{20a}$$

or

$$\epsilon = \frac{\pi^2 w_o^2}{2\ell^2} \cdot \sum_{N=1,3,5}^{\infty} N^2 A_N^2 \cos^2\frac{N\pi x}{\ell} \tag{20b}$$

The plastic strain energy equals the yield force times the strain integrated over the length:

$$U = \frac{\pi^2 F_y w_o^2}{\ell^2} \sum_{N=1,3,5}^{\infty} N^2 A_N^2 \int_0^{\ell/2} \cos^2\left(\frac{N\pi x}{\ell}\right) dx \tag{21}$$

or, after integrating:

$$U = \frac{\pi^2 F_y w_o^2}{4\ell} \sum_{N=1,3,5}^{\infty} N^2 A_N^2 \tag{22}$$

If the loading is a quasi-static pressure of intensity p, then the work is given by the previously obtained Eq. (7). We again use the Rayleigh-Ritz method to obtain amplitudes of the different modes. Although our system is not conservative, it is linear because we have chosen to consider rigid-perfectly plastic material behavior over the full range of deformation. Proceeding as before by taking the difference in the strain energy and work, we have

$$(U - wk) = \frac{\pi^2 F_y w_o^2}{4\ell} \sum_{N=1,3,5}^{\infty} N^2 A_N^2 - \frac{2pbw_o\ell}{\pi} \sum_{N=1,3,5}^{\infty} \frac{A_N}{N} \tag{23}$$

Differentiating with respect to A_N and setting the result equal to zero yields for A_N:

$$A_N = \left(\frac{4pb\ell^2}{\pi^3 F_y w_o}\right)\frac{1}{N^3} \tag{24}$$

---

*A string is defined here as an element with negligible bending stiffness.

Hence, the amplitude of various modes relative to the first one is

$$\frac{A_N}{A_1} = \frac{1}{N^3} \tag{25}$$

If we now proceed with a dynamic solution, the deformed shape for a three mode solution is given by:

$$y = mw_o \left[\sin\frac{\pi x}{\ell} + \frac{1}{27}\sin\frac{3\pi x}{\ell} + \frac{1}{125}\sin\frac{5\pi x}{\ell} \right] \tag{26}$$

The parameter m equals 1.0299 because y is equal to w_o at mid-span. Substituting into Eq. (20a) gives as an approximation for the strain:

$$\epsilon = 1.0607 \left[\frac{\pi^2 w_o^2}{2\ell^2}\right] \left[\cos\frac{\pi x}{\ell} + \frac{1}{9}\cos\frac{3\pi x}{\ell} + \frac{1}{25}\cos\frac{5\pi x}{\ell} \right]^2 \tag{27}$$

The plastic strain energy is

$$U = 2 \int_0^{\ell/2} F_y \, \epsilon \, dx \tag{28a}$$

or

$$U = 1.0607 \left[\frac{\pi^2 F_y w_o^2}{\ell^2}\right] \int_0^{\ell/2} \left[\cos\frac{\pi x}{\ell} + \frac{1}{9}\cos\frac{3\pi x}{\ell} + \frac{1}{25}\cos\frac{5\pi x}{\ell} \right]^2 dx \tag{28b}$$

Performing the desired integration yields:

$$U = 1.221 \left[\frac{\pi^2 F_y w_o^2}{4\ell}\right] \tag{29}$$

The work which must be equated to this strain energy is given by:

$$wk = 2pb(1.0299w_o) \int_0^{\ell/2} \left[\sin\frac{\pi x}{\ell} + \frac{1}{27}\sin\frac{3\pi x}{\ell} + \frac{1}{125}\sin\frac{5\pi x}{\ell} \right] dx \tag{30}$$

or, after integrating,

$$wk = 1.0443 \left[\frac{2pbw_o\ell}{\pi}\right] \tag{31}$$

16

Equating the work to the strain energy and solving for a nondimensionalized mid-span deformation, w_o/ℓ, gives:

$$\frac{w_o}{\ell} = 0.8553 \left[\frac{8pb\ell}{\pi^3 F_y}\right]$$ (32)

This plastic extensional solution is not as exact using only one mode as the elastic bending solution. Nevertheless, the deformation is predicted to within 15 percent, and the single mode does overestimate the deformation. The maximum strains can also be compared. This maximum occurs at $x = 0$. Substituting Eq. (32) into Eq. (27) and setting $x = 0$ gives for the maximum strains:

$$\epsilon_{max} = 1.0282 \left(\frac{32p^2 b^2 \ell^2}{\pi^4 F_y^2}\right)$$ (33)

As is seen in Eq. (33), the strain is predicted fairly accurately using a one mode approximation. The difference between a one mode (the first) and a three mode approximation is less than 3 percent. Considering the mathematical complexities which are introduced by adding more modes, the additional effort is probably not worth it.

2. Influence of Other Shapes

To illustrate the influence of assumed deformed shape on results, we analyzed elastic bending and plastic bending of simply-supported beams loaded with a uniform impulse. Examples of these solutions are given in Part C of this section and will not be repeated here. Equations are summarized in Chapter III.

For an elastic analysis, we evaluate computed results for three different deformed shapes. The first shape is a parabola, the second is the first mode sine wave, and the third shape is the static one for a uniformly applied load. Because each of these deformation patterns must satisfy the essential boundary conditions of a simply-supported beam, they will be similar in shape. Nevertheless they represent three distinct deformation patterns.

All three solutions give similar results for the strain energy U, the maximum deformation w_o, and the maximum strain ϵ_{max}, as can be observed in Table I. The results in Table I have been nondimensionalized so numerical coefficients can be compared directly. Only the numerical coefficient differs slightly in all of these solutions. Both the first mode and static deformed shape approximations yield the same answer to within a few percent.

The second group of illustrations includes plastic bending in a beam loaded dynamically with a uniform impulse. One more deformed shape will be added to the results for the three elastic shapes. The fourth shape is a static hinge yielding plastically in the center of the beam while the rest of the beam remains rigid. This deformed shape is a common one in civil engineering applications. Whereas the other three deformed shapes distribute the deformation, the stationary hinge concentrates the deformation. Table II compares non-dimensionalized numerical coefficients for strain energy, maximum plastic deformation, and maximum plastic strain for these four different deformed shapes.

17

Parameter \\ Deformed Shape $\frac{y}{w_0}=$	Parabola $4\left(\frac{x}{\ell}\right)^2$	First Mode $\sin\left(\frac{\pi x}{\ell}\right)$	Static Deformed Shape $\frac{16}{5}\left[\left(\frac{x}{\ell}\right)-2\left(\frac{x}{\ell}\right)^3+\left(\frac{x}{\ell}\right)^4\right]$
Strain Energy $\dfrac{U\ell^3}{EbH^3 w_0^2}=$	2.666	2.029	2.048
Deformation $\dfrac{w_0\sqrt{\rho E}\,H^2}{i\ell^2}=$	0.4330	0.4964	0.4941
Strain $\dfrac{\epsilon_{max}\sqrt{\rho E}\,H}{i}=$	1.732	2.449	2.372

TABLE II. IMPULSIVE BENDING SOLUTION FOR A SIMPLY-SUPPORTED PLASTIC BEAM

Parameter \\ Deformed Shape $\frac{y}{w_0}$	Parabola $4\left(\frac{x}{\ell}\right)^2$	First Mode $\sin\left(\frac{\pi x}{\ell}\right)$	Static Deformed Shape $\frac{16}{5}\left[\left(\frac{x}{\ell}\right)-2\left(\frac{x}{\ell}\right)^3+\left(\frac{x}{\ell}\right)^4\right]$	Stationary Hinge $2\left(\frac{x}{\ell}\right)$ for $0\leq\frac{x}{\ell}\leq\frac{1}{2}$
Strain Energy $\dfrac{U\ell}{\sigma_y w_0 bH^2}=$	2.00	1.571	1.60	1.00
Deformation $\dfrac{w_0\rho\sigma_y H^3}{i^2\ell^2}=$	0.250	0.3183	0.3125	0.500
Strain $\dfrac{\epsilon_{max}\rho\sigma_y H^2}{i^2}=$	1.00	1.571	1.500	No Meaning

In the plastic beam, the first mode and static deformed shape give deformations and strains which are close to one another. The stationary hinge yields no rational estimate for strain because there is no gauge length associated with a concentrated hinge. The deformation is also much larger for a stationary hinge than comparable deformations from distributed deformed shapes. A concentrated hinge yields much too small a strain energy and too large a deformation. Distributed deformed shapes are much closer to reality and give more accurate predictions.

As these illustrations show, either a first mode approximation or a static deformed shape is a good approximation. We would recommend a first mode approximation for symmetric deformations, as in simply-supported and clamped-clamped beams, because the resulting algebra is slightly easier. For nonsymmetric responses, as in a simply-supported clamped beam, the static deformed shape should be used. If the static deformed shape is not used in nonsymmetric cases, uncertainty will otherwise exist.

In all of the illustrations, the assumed deformed shape being applied to a solution is of less importance to the resulting deformations and strains than the effects of coupling. Supporting a flexible structural component on a flexible foundation has a much greater influence on structural response than the assumed deformed shape, as the next part of this section shows.

B. Energy Solutions for Coupled Rigid-Plastic Systems

In the suppressive structures program, energy solutions have been difficult to apply because the actual structure is a combination of plates and beams or a combination of I-beams and hoops, rather than a simple beam, plate, or membrane configuration. Although energy solutions developed to date in the Suppressive Structures Program (see Refs. 1, 4, 6, and 9) apply for simple structural elements, structural configurations which are combinations of elements can also be solved using this approach; however, to complete such a solution, one more equation is needed to couple deformation in the first structural element with deformation in the second. For a rigid-plastic system, derivation of the required relationship is straightforward.
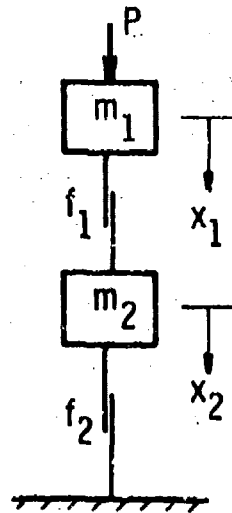
FIGURE 1. RIGID-PLASTIC
RHEOLOGICAL MODEL

Coupled plastic systems can be visualized by a rigid-plastic, rheological model as in Figure 1. In Figure 1, the yield force f_1 must exceed the yield force f_2, and the quasi-static force P must be less than both f_1 and f_2; otherwise, the system will not act as a coupled system. The relative residual deformation $(X_1 - X_2)$ is related to the residual deformation X_2 through an impedance match involving the parameters m_1, m_2, f_1, f_2, and P. Equation (34) is this coupling relationship.

$$\frac{(X_1 - X_2)}{X_2} = \frac{m_2(f_2 - P)}{m_1(f_1 - f_2)} \tag{34}$$

To complete an energy solution, one now only has to equate the kinetic energy to the strain energy or the maximum possible work to the strain energy to obtain estimates for the deformation in a dynamically loaded suppressive shield. In a coupled system as in Figure 1, the strain energy is given by:

$$S.E. = f_1(X_1 - X_2) + f_2(X_2) \tag{35}$$

Because two equations now exist for X_1 and X_2, they can be solved simultaneously. We will proceed by developing Eq. (34) and illustrating its use in two example problems.

19

1. Development of the Coupling Equation

Assume m_1 is hit simultaneously with an impulse I and a quasi-static force P. Then the two equations of motion are:*

$$m_1 \ddot{x}_1 + f_1 = P \tag{36a}$$

$$m_2 \ddot{x}_2 + f_2 = f_1 \tag{36b}$$

For no initial displacement, no initial velocity for m_2, and an initial velocity of I/m_1 for m_1, we obtain by direct integration:

$$x_1 = \frac{It}{m_1} - \frac{f_1 t^2}{2m_1} + \frac{Pt^2}{2m_1} \tag{37a}$$

$$x_2 = \frac{(f_1 - f_2)t^2}{2m_2} \tag{37b}$$

Coupled motion continues until $(\dot{x}_1 - \dot{x}_2)$ equals zero,

$$\left(\frac{dx_1}{dt} - \frac{dx_2}{dt}\right) = 0 = \frac{I}{m_1} - \left(\frac{f_1}{m_1} + \frac{f_1}{m_2}\right) t' + \frac{f_2}{m_2}t' + \frac{P}{m_1}t' \tag{38}$$

or until time t' given by

$$t' = \frac{m_2 I}{[(m_1 + m_2)f_1 - m_1 f_2 - m_2 P]} \tag{39}$$

At this time, the new initial conditions for m_2 are:

$$x_2' = \frac{m_2(f_1 - f_2)I^2}{2[(m_1 + m_2)f_1 - m_1 f_2 - m_2 P]^2} \tag{40a}$$

$$\frac{dx_2'}{dt} = \frac{(f_1 - f_2)I}{[(m_1 + m_2)f_1 - m_1 f_2 - m_2 P]} \tag{40b}$$

The relative motion $(x_1' - x_2')$ equals the maximum relative residual motion $(X_1 - X_2)$

$$(X_1 - X_2) = \frac{m_2 I^2}{2m_1 [(m_1 + m_2)f_1 - m_1 f_2 - m_2 P]} \tag{41}$$

After element f_1 "locks up" at time t', motion continues as an uncoupled system. The equation of motion in this second phase is given by:

---

*Note that I is *total* impulse with dimensions of FT, rather than specific blast impulse i with dimensions of FT/L^3.

$$(m_1 + m_2)\ddot{x}_2 + f_2 = P \tag{42}$$

By establishing a new time zero at the instant t^* when the motion becomes uncoupled, using the initial conditions given by Eqs. (40), and integrating, we obtain as the equation for displacement in the second phase:

$$x_2 = \frac{-(f_2 - P)t^2}{2(m_1 + m_2)} + \frac{(f_1 - f_2)lt}{[(m_1 + m_2)f_1 - m_1 f_2]} + \frac{m_2(f_1 - f_2)l^2}{2[(m_1 + m_2)f_1 - m_1 f_2]^2} \tag{43}$$

All motion stops at time $t\dagger$ given by:

$$t\dagger = \frac{(m_1 + m_2)(f_1 - f_2)l}{(f_2 - P)[(m_1 + m_2)f_1 - m_1 f_2 - m_2 P]} \tag{44}$$

Substituting $t\dagger$ into Eq. (43) and gathering terms gives the maximum residual deformation, X_2, for element m_2.

$$X_2 = \frac{(f_1 - f_2)l^2}{2(f_2 - P)[(m_1 + m_2)f_1 - m_1 f_2 - m_2 P]} \tag{45}$$

Finally, dividing Eq. (41) by Eq. (45) gives the relative displacement coupling equation already presented as Eq. (34).

$$\frac{(X_1 - X_2)}{X_2} = \frac{m_2(f_2 - P)}{m_1(f_1 - f_2)} \tag{34}$$

This equation is the key coupling relationship which will be used in all calculations. Use of the equation is best illustrated by some example problems. Calculation of the mass m for a structural component is no problem; however, the effective force f requires assumptions when calculated for a beam or plate element. We will calculate the force f by assuming a deformed shape for a structural component, calculating the strain energy stored in that deformed shape, determining the average deformation for a given deformed shape, and finally dividing the strain energy by the average deformation. Once this procedure is complete, the coupling Eq. (34) and energy relationships permit structural deformations and strains to be determined in a procedure similar to that used in any uncoupled structural analysis.

2. Application to the Category I Shield

The Category I shield is used as the approximate illustrative example because it was the first to draw our attention to the need for a coupled solution. Here we will derive the equations for coupled response of the beams and rings. In Chapter IV, comparisons with data from the Category I 1/4-scale model demonstrate the validity of the coupled energy solution.

Basically, this shield is a barrel as shown in Figure 5 (page 52). External circular hoops provide restraint for longitudinal I-beams. The I-beams represent the $m_1 - f_1$ structure, and the hoops are the $m_2 - f_2$ structure. We will treat the I-beams as clamped-clamped beams. An assumed deformation pattern for this structural component is given by:

21

$$y = \frac{w_o}{2} \left(1 + \cos \frac{2\pi x}{\ell}\right) \qquad (46)$$

where

w_o = maximum mid-span deformation relative to the supports

ℓ = total span

x = coordinate system with origin at mid-span

y = deformation at some value of x

Differentiating Eq. (46) twice gives:

$$\frac{d^2 y}{dx^2} = \frac{-2\pi^2 w_o}{\ell^2} \cos \frac{2\pi x}{\ell} \qquad (47)$$

The strain Energy $\text{S.E.}_①$ is given by the integral

$$\text{S.E.}_① = 2 \int_0^{\ell/2} M_y \frac{d^2 y}{dx^2} dx \qquad (48)$$

where

M_y = plastic yield moment

Substituting Eq. (47) into Eq. (48) and completing the desired integration gives:

$$\text{S.E.}_① = \frac{4\pi M_y w_o}{\ell} \qquad (49)$$

The average deformation y_{AVG} must be calculated next. It is obtained by the integral

$$[\ell] y_{AVG} = 2 \int_0^{\ell/2} \frac{w_o}{2} \left(1 + \cos \frac{2\pi x}{\ell}\right) dx \qquad (50)$$

or

$$y_{AVG} = \frac{w_o}{2} \qquad (51)$$

The force f_1 in one beam equals $\text{S.E.}_①$ divided by the average deformation, or:

$$f_1 = \frac{8\pi M_y}{\ell} \qquad (52)$$

22

The mass m_1 equals:

$$m_1 = \rho_b A_b \ell \tag{53}$$

where

ρ_b = mass density of a beam

A_b = cross-sectional area of a beam

Next, f_2 and m_2 must be calculated for the hoops. If we assume hoops of equal effective cross-sectional area, A_h, on each end, the deformation will be a symmetric change in radius ΔR. The strain energy for both hoops is:

$$\text{S.E.}_{\textcircled{2}} = (2\sigma_y) \left(\frac{\Delta R}{R}\right) (2\pi R A_h) \tag{54a}$$

or

$$\text{S.E.}_{\textcircled{2}} = 4\pi\sigma_y A_h \Delta R \tag{54b}$$

The average deflection in a hoop is the deflection ΔR. This means that the force f_2 is given by:

$$f_2 = \text{S.E.}_{\textcircled{2}} / \Delta R \tag{55a}$$

or

$$f_2 = 4\pi\sigma_y A_h \tag{55b}$$

The mass m_2 equals twice the mass density times the area times the circumference, or:

$$m_2 = (2\rho_h)(A_h)(2\pi R) \tag{56a}$$

or

$$m_2 = 4\pi\rho_h A_h R \tag{56b}$$

The quasi-static force P equals the pressure p times the internal circumference times the length, or:

$$P = (p)(2\pi r)(\ell) \tag{57a}$$

$$p = 2\pi r \ell p \tag{57b}$$

Now the coupling equation can be used to relate the average deformation in the beams $(w_o/2)$ to the deformation in the hoops ΔR. Substituting for m_1, m_2, f_1, f_2, and P then yields:

23

$$\frac{\frac{w_o}{2}}{\Delta R} = \frac{(4\pi\rho_h A_h R)[(4\pi\sigma_h A_h) - 2\pi r\ell p]}{(N\rho_b A_b \ell)\left(\dfrac{8\pi N\sigma_b z}{\ell} - 4\pi\sigma_h A_h\right)} \tag{58}$$

The parameter N stands for the number of beams. The mass of the beams and force equals N times m_1 or f_1, respectively, for a single beam in Eq. (58). In addition, the yield stress σ_b times the plastic section modulus z was substituted for the yield moment in the beam force equation, Eq. (52). Reducing Eq. (58) algebraically gives the ratio for the maximum deformation in the beams relative to the change in hoop radius.

$$\frac{w_o}{\Delta R} = \frac{8\pi\left(\dfrac{\rho_h A_h R}{N\rho_b A_b \ell}\right)\left(1 - \dfrac{pr\ell}{2\sigma_h A_h}\right)}{\left[2\left(\dfrac{N\sigma_b z}{\sigma_h A_h \ell}\right) - 1\right]} \tag{59}$$

The solution proceeds by writing the strain energy S.E. for the entire system. This energy equals the sum of Eqs. (49) and (54), or:

$$\text{S.E.} = \frac{4\pi N\sigma_b z w_o}{\ell} + 4\pi\sigma_h A_h \Delta R \tag{60}$$

Substituting Eq. (59) for ΔR in Eq. (60) gives:

$$\text{S.E.} = \frac{4\pi N\sigma_b z w_o}{\ell} + \frac{N\rho_b A_b \sigma_h \ell w_o}{2\rho_h R} \frac{\left[2\left(\dfrac{N\sigma_b z}{\sigma_h A_h \ell}\right) - 1\right]}{\left(1 - \dfrac{pr\ell}{2\sigma_h A_h}\right)} \tag{61}$$

Next the energy imparted to the structure must be estimated. This energy comes from the kinetic energy imparted through blast waves and the work from the quasi-static pressure buildup within a suppressive shield. Algebraically, this energy E_N equals Eq. (62) with loads imparted to the beams.

$$E_N = \frac{NI^2}{2m_1} + pb\ell(y_{\text{AVG}} + \Delta R) \tag{62}$$

where

b = loaded width of the beams.

Substituting for I, m_1, y_{AVG}, and Eq. (59) for ΔR yields, after collecting terms:

$$E_N = \frac{Ni^2 b^2 \ell}{2\rho_b A_b} + \frac{pb\ell w_o}{2} \left[1.0 + \frac{N\rho_b A_b \ell}{4\pi\rho_h A_h R} \frac{\left(\frac{2N\sigma_b z}{\sigma_h A_h \ell} - 1 \right)}{\left(1 - \frac{pr\ell}{2\sigma_h A_h} \right)} \right] \tag{63}$$

Finally, equating E_N, Eq. (63), to S.E., Eq. (61), and gathering terms yields an equation which can be solved for w_o, the maximum deflection in the beams.

$$\frac{i^2 b^2 \ell^2}{\rho_b A_b \sigma_b z w_o} + \frac{pb\ell^2}{N\sigma_b z} \left[1.0 + \frac{N\rho_b A_b \ell}{4\pi\rho_h A_h R} \frac{\left(\frac{2N\sigma_b z}{\sigma_h A_h \ell} - 1 \right)}{\left(1 - \frac{pr\ell}{2\sigma_h A_h} \right)} \right] = 8\pi + \frac{\sigma_h \rho_b A_b \ell^2}{\sigma_b \rho_h z R} \frac{\left(\frac{2N\sigma_b z}{\sigma_h A_h \ell} - 1 \right)}{\left(1 - \frac{pr\ell}{2\sigma_n A_h} \right)} \tag{64}$$

Equation (64) yields w_o, the maximum beam deformation relative to the rings, and subsequent substitution in Eq. (59) yields ΔR, the change in hoop radius. Strains can also be estimated. The residual hoop strain equals $\Delta R/R$ as in Eq. (65a), and the maximum residual bending strain in the beams equals half the beam depth $H/2$ times the maximum beam curvature as given by Eq. (47). Equation (65b) is the maximum residual strain in the beams.

$$\epsilon_{\text{hoop}} = \frac{\Delta R}{R} \tag{65a}$$

$$\epsilon_{\text{beams}} = \frac{\pi^2 w_o H}{\ell^2} \tag{65b}$$

Refer to Chapter IV for calculations based on these equations for the 1/4-scale model of the Category I shield.

3. *Application to the Category III Shield*

The second example will be that of a rectangular membrane, supported rigidly along two opposite edges and by flexible clamped-clamped beams along the other two edges. This configuration might be representative of the original Category III containment structure[19] which was replaced by the 1/4-scale Category I shield. We begin by assuming a deformed shape for the membrane, Eq. (66).

$$w = w_o \cos \frac{\pi x}{2X} \cos \frac{\pi y}{2Y} \tag{66}$$

In a membrane the strains are calculated from the first derivatives of the slope by:

$$\epsilon_{XX} = \frac{1}{2} \left(\frac{\partial w}{\partial x} \right)^2 = \frac{\pi^2 w_o^2}{8X^2} \sin^2 \left(\frac{\pi x}{2X} \right) \cos^2 \left(\frac{\pi y}{2Y} \right) \tag{67a}$$

25

$$\epsilon_{yy} = \frac{1}{2}\left(\frac{\partial w}{\partial y}\right)^2 = \frac{\pi^2 w_o^2}{8Y^2}\cos^2\left(\frac{\pi x}{2X}\right)\sin^2\left(\frac{\pi y}{2Y}\right) \tag{67b}$$

$$\epsilon_{xy} = \left(\frac{\partial w}{\partial x}\right)\left(\frac{\partial w}{\partial y}\right) = \frac{\pi^2 w_o^2}{16XY}\sin\left(\frac{\pi x}{X}\right)\sin\left(\frac{\pi y}{Y}\right) \tag{67c}$$

In a structure under a biaxial state of stress, the strain energy per unit volume is given by the integral:

$$\frac{S.E.①}{Vol.} = \int\left[\sigma_{xx}\,d\epsilon_{xx} + 2\sigma_{xy}\,d\epsilon_{xy} + \sigma_{yy}\,d\epsilon_{yy}\right] \tag{68}$$

If we assume a rigid-plastic material with a yield point in the plate σ_p, then $\sigma_{xx} = \sigma_{yy} = \sigma_p$ and $\sigma_{xy} = \sigma_p/\sqrt{3}$ according to the distortion energy yield theory. Substitution of constant stresses into Eq. (68), integrating Eq. (68) for strains, substituting the strains from Eqs. (67) into Eq. (68), and expressing the volume of the membrane through the thickness times a double integral yields:

$$S.E.① = 4\int_0^X dx \int_0^Y dy\left[\sigma_p h\frac{\pi^2 w_o^2}{8X^2}\sin^2\left(\frac{\pi x}{2X}\right)\cos^2\left(\frac{\pi y}{2Y}\right)\right.$$

$$+ \frac{2\sigma_p h}{\sqrt{3}}\frac{\pi^2 w_o^2}{16XY}\sin\left(\frac{\pi x}{X}\right)\sin\left(\frac{\pi y}{Y}\right) + \frac{\sigma_p h\pi^2 w_o^2}{8Y^2} \tag{69}$$

$$\left. \times \cos^2\left(\frac{\pi x}{2X}\right)\sin^2\left(\frac{\pi y}{2Y}\right)\right]$$

Performing the required double integration gives:

$$S.E.① = \frac{\pi^2\sigma_p h w_o^2}{8}\left[\frac{Y}{X} + \frac{16}{\sqrt{3}\pi^2} + \frac{X}{Y}\right] \tag{70}$$

The average plate deformation must be calculated next by double integration.

$$(4XY)w_{AVG} = 4\int_0^X dx \int_0^Y dy\, w_o\cos\frac{\pi x}{2X}\cos\frac{\pi y}{2Y} \tag{71}$$

or:

$$w_{AVG} = \frac{4w_o}{\pi^2} \tag{72}$$

26

The force f_1 in a plate equals S.E.(1) divided by w_{AVG}, or:

$$f_1 = \frac{\pi^4 \sigma_p h w_o}{32} \left[\frac{Y}{X} + \frac{16}{\pi^2 \sqrt{3}} + \frac{X}{Y} \right] \tag{73}$$

The mass m_1 equals:

$$m_1 = 4\rho_p h X Y \tag{74}$$

Next, f_2 and m_2 must be calculated; however, this has already been done in the first example. Because there are two beams, the quantity f_2 equals twice f in Eq. (52), and the mass m_2 equals twice m in Eq. (53). These results are summarized as Eqs. (75).

$$f_2 = \frac{16\pi M_y}{\ell} \tag{75a}$$

$$m_2 = 2\rho_b A \ell \tag{75b}$$

The average deflection of the beams is still $w_b/2$, and the quasi-static force is given by Eq. (76).

$$P = 4pXY \tag{76}$$

We are now prepared to substitute into Eq. (34). Substituting for m_1, m_2, f_1, f_2, and P yields the coupling equation for deflections.

$$\frac{8w_p}{\pi^2 w_b} = \frac{32\pi \rho_b M_y A - 8\rho_b p X Y A \ell}{4\rho_p h X Y \left[\frac{\pi^4 \sigma_p h w_p}{32} \left\{ \frac{Y}{X} + \frac{16}{\sqrt{3}\pi^2} + \frac{X}{Y} \right\} - \frac{16\pi M_y}{\ell} \right]} \tag{77}$$

or:

$$w_b = \frac{\frac{\pi}{32} \frac{\rho_p \sigma_p h^2 X Y w_p^2}{\rho_b m_y A} \left\{ \frac{Y}{X} + \frac{16}{\sqrt{3}\pi^2} + \frac{X}{Y} \right\} - \frac{16}{\pi^2} \frac{\rho_p h X Y w_p}{\rho_b A \ell}}{\left(1 - \frac{p X Y \ell}{4 M_y} \right)} \tag{78}$$

The solution proceeds by writing the strain energy S.E. for the entire system. This energy is two times Eq. (49) for the strain energy in one beam plus Eq. (70).

$$\text{S.E.} = \frac{8\pi M_y w_b}{\ell} + \frac{\pi^2 \sigma_p h w_p^2}{8} \left[\frac{Y}{X} + \frac{16}{\sqrt{3}\pi^2} + \frac{X}{Y} \right] \tag{79}$$

Substituting Eq. (78) for w_b and collecting terms yields:

$$S.E. = \frac{\pi^2 \sigma_p h w_p^2}{8} \left[1 + \frac{2\rho_p XYh}{\rho_b A\ell \left(1 - \frac{pXY\ell}{4M_y}\right)}\right]\left[\frac{Y}{X} + \frac{16}{\sqrt{3\pi^2}} + \frac{X}{Y}\right]$$

$$- \frac{128\rho_p M_y XYhw_p}{\pi\rho_b A\ell^2 \left(1 - \frac{pXY\ell}{4M_y}\right)} \tag{80}$$

The kinetic energy from the blast wave which is imparted to the system equals:

$$KE = \frac{i^2(4XY)^2}{2(4\rho_p XYh)} = \frac{2i^2 XY}{\rho_p h} \tag{81}$$

The work from the quasi-static pressure loading equals:

$$WK = p(4XY)\left(\frac{4}{\pi^2}w_p + \frac{1}{2}w_b\right) \tag{82}$$

Or after substituting Eq. (78) for w_b:

$$WK = 2pXYw_p\left[\frac{8}{\pi^2} + \frac{\pi\rho_p\sigma_p h^2 XYw_p\left(\frac{Y}{X} + \frac{16}{\sqrt{3\pi^2}} + \frac{X}{Y}\right)}{32\rho_b M_y A\left(1 - \frac{pXY\ell}{4M_y}\right)} - \frac{16\rho_p hXY}{\pi^2\rho_b A\ell\left(1 - \frac{pXY\ell}{4M_y}\right)}\right] \tag{83}$$

Equating WK + KE to S.E. gives the final solution. In nondimensional format this solution is:

$$\pi_l + \pi_p\left[0.8106\pi_w + \frac{0.3927\pi_p\pi_\sigma\pi_y\pi_w^2}{(4 - \pi_\sigma\pi_p)} - \frac{6.484\pi_p\pi_w}{(4 - \pi_\sigma\pi_p)}\right] = 0.6169$$

$$\times \left[1 + \frac{3\pi_p}{(4 - \pi_\sigma\pi_p)}\right]\pi_y\pi_w^2 - 81.48\frac{\pi_p\pi_w}{\pi_\sigma(4 - \pi_\sigma\pi_\sigma)} \tag{84a}$$

where

$$\pi_\rho = \frac{\rho_p XYh}{\rho_b A\ell} \tag{84b}$$

$$\pi_\sigma = \frac{\sigma_p h^2 \ell}{M_y}$$

$$\pi_p = \frac{p_R XY}{\sigma_p h^2}$$

$$\pi_i = \frac{i^2 XY}{\rho_p \sigma_p h^4}$$

(84b)
(Concl)

$$\pi_y = \frac{Y}{X} + \frac{16}{\sqrt{3\pi^2}} + \frac{X}{Y}$$

$$\pi_w = \frac{w_p}{h}$$

Equation (84) is a quadratic equation that must be solved for π_y or w_p. After w_p is obtained, w_b is obtained from Eq. (78), which in nondimensional format is:

$$\frac{w_b}{w_p} = \frac{0.3927\pi_p \pi_\sigma \pi_y \pi_w - 6.484\pi_p}{(4 - \pi_\sigma \pi_p)}$$

(85)

To complete this illustration, let us apply Eqs. (84) and (85) to the Category III shield. We will assume parameters as follows:

p = 66 psi

i = 0.179 psi-sec

X = 26.5 in.

Y = 56.5 in.

h = 1.033 in. (this is an effective thickness)

$\rho_p = \rho_b = 7.33 \times 10^{-4} \dfrac{\text{lb-sec}^2}{\text{in.}^4}$

$\sigma_p = \sigma_b$ = 48,000 psi

A = 61.71 in.^{2}

ℓ = 113 in.

$M_y = 1.21 \times 10^{+7}$ in.-lb

Substitution of these parameters into the π terms gives:

$$\pi_p = 0.2218$$

$$\pi_o = 0.4783$$

$$\pi_p = 1.929$$

$$\pi_i = 1.197$$

$$\pi_y = 3.537$$

Substituting into Eq. (84) gives a positive root for π_w of 3.953; hence, $w_p = 4.083$ inches. Finally, substitution into Eq. (85) gives $w_b = -1.135$ inches. This negative sign associated with w_b is not a mistake. It means that the plate and beam systems are not coupled as has been assumed; hence, this analysis is not appropriate for the parameters substituted into it. In this particular solution, f_2 is greater than f_1. This means there is no plastic deformation in the second element, and the particular system under investigation is uncoupled. Appropriate answers can be obtained by using uncoupled techniques which have already been presented. The purpose of this second illustration was to emphasize the meaning of a negative sign when it is encountered in this type of analysis.

4. Importance of Treating Coupled Response

We have shown that energy solutions are possible for coupled perfectly plastic systems. For two members in a coupled system, one additional equation is needed to relate deflections in the first member to deflections in the second member. Equation (34) is presented as a relationship for coupling the deflections. With the assistance of this one extra equation, energy solutions can be developed as in any rigid-plastic coupled system.

In Chapter IV we will show that the effect of coupling is very important for predicting response in the Category I shield. On the other hand, the example above shows that coupling is unimportant for predicting membrane deformations in the Category III shield. While these solutions are more complicated than uncoupled solutions, residual deflections and strains for coupled systems can be predicted with closed-form algebraic solutions, and the usefulness of the approximate energy methods for predicting response to blast or impact loading is greatly enhanced.

C. Elastic-Plastic Energy Solutions for Beams

In the design of suppressive shields we are usually interested in predicting onset of failure, and hence maximum strain or maximum stress. In most problems, a beam has segments which remain elastic and segments which go plastic. The assumptions of total elasticity or total plasticity throughout all elements in a structural component, or concentrated plasticity in a hinge, are approximations. To obtain an idea of how elastic-plastic solutions could be presented to designers, and to see how combined solutions might be obtained from simple elastic and/or simple plastic solutions, two elastic-plastic solutions have been developed for a simply-supported beam and a string.

30

The constitutive relationship used for both solutions is given by Eq. (86).

$$\sigma = \sigma_y \tanh \frac{E\epsilon}{\sigma_y} \qquad (86)$$

This is an excellent approximation to an elastic-plastic material. For small strains, $E\epsilon/\sigma_y < 0.5$, the stress-strain curve is a linear one with $\sigma = E\epsilon$; and, for large strains, $E\epsilon/\sigma_y > 2.0$, the stress-strain curve is a perfectly plastic one, with $\sigma = \sigma_y$.

1. Solution for a Simply-Supported Beam

In any structural element under a uniaxial state of stress, the strain energy per unit volume is given by:

$$\frac{U}{\text{Vol.}} = \int \sigma \, d\epsilon \qquad (87)$$

If we substitute Eq. (86) for σ and integrate from a strain of zero to the maximum strain ϵ, we obtain:

$$\frac{U}{\text{Vol.}} = \int_0^\epsilon \sigma_y \tanh\left(\frac{E\epsilon}{\sigma_y}\right) d\epsilon \qquad (88)$$

Or:

$$\frac{U}{\text{Vol.}} = \frac{\sigma_y^2}{E} \ln \cosh\left(\frac{E\epsilon}{\sigma_y}\right) \qquad (89)$$

Equation (89) is then applied to any bending or extensional solution by substituting the strain and integrating over the volume. If we use the assumed deformed shape for a simply-supported beam given by the first term of Eq. (1), the strain ϵ for a differential element in bending is:

$$\epsilon = -h \frac{d^2 y}{dx^2} = \frac{\pi^2 w_o h}{\ell^2} \sin \frac{\pi x}{\ell} \qquad (90)$$

If the beam is of rectangular cross section, the volume equals:

$$\text{Vol.} = 4b \int_0^{H/2} dh \int_0^{\ell/2} dx \qquad (91)$$

Substituting the expression for ϵ and the volume integral into Eq. (89) gives the following double integration for the strain energy U.

$$U = \frac{4\sigma_y^2 b}{E} \int_0^{H/2} \int_0^{\ell/2} \ln \cosh\left(\frac{\pi^2 w_o E h}{\sigma_y \ell^2} \sin \frac{\pi x}{\ell}\right) dh \, dx \qquad (92)$$

or

$$U = \frac{4\sigma_0^2 bH\ell}{\pi^2 E} \int_0^{\pi/2} \int_0^{\pi/2} \ell n \cosh\left[\left(\frac{\pi w_o HE}{\sigma_y \ell^2}\right) \beta \sin \alpha\right] d\beta \, d\alpha \tag{93a}$$

where

$$\alpha = \pi x/\ell \text{ and } \beta = \pi h/H. \tag{93b}$$

Next we assume that the loading is a uniformly applied impulse, giving for the kinetic energy:

$$KE = \frac{I^2}{2m} = \frac{i^2 b\ell}{2\rho H} \tag{94}$$

Equating the kinetic energy to the strain energy and rearranging yields the dimensionless equation:

$$\left(\frac{\pi^2 i^2 E}{8\rho\sigma_y^2 H^2}\right) = \int_0^{\pi/2} \int_0^{\pi/2} \ell n \cosh\left[\left(\frac{\pi w_o HE}{\sigma_y \ell^2}\right) \beta \sin \alpha\right] d\beta \, d\alpha \tag{95}$$

This equation can be written as:

$$C = \int_0^{\pi/2} \int_0^{\pi/2} \ell n \cosh\left[D\beta \sin \alpha\right] d\beta \, d\alpha \tag{96a}$$

where

$$C = (\pi^2 i^2 E/8\rho\sigma_y^2 H^2) \text{ and } D = (\pi w_o HE/\sigma_y \ell^2) \tag{96b}$$

A computer program was required to numerically perform the double integration. Results of this program are represented by the solid continuous line in Figure 2. Dashed lines in the figure are the asymptotes for completely elastic or fully plastic behavior. Note that the elastic-plastic solution correctly approaches the elastic asymptote for small deformations and the plastic asymptote for large deformations.

2. *String Solution*

The string solution uses the same strain energy per unit volume equation, Eq. (89), as the beam solution. These solutions differ in the equations relating strain to deformation. In an extensional element the strain is given by Eq. (20a). Substituting the first term of Eq. (1) for the assumed deformed shape in Eq. (20a) gives Eq. (97).

$$\epsilon = \frac{\pi^2 w_o^2}{2\ell^2} \cos^2\left(\frac{\pi x}{\ell}\right) \tag{97}$$

32
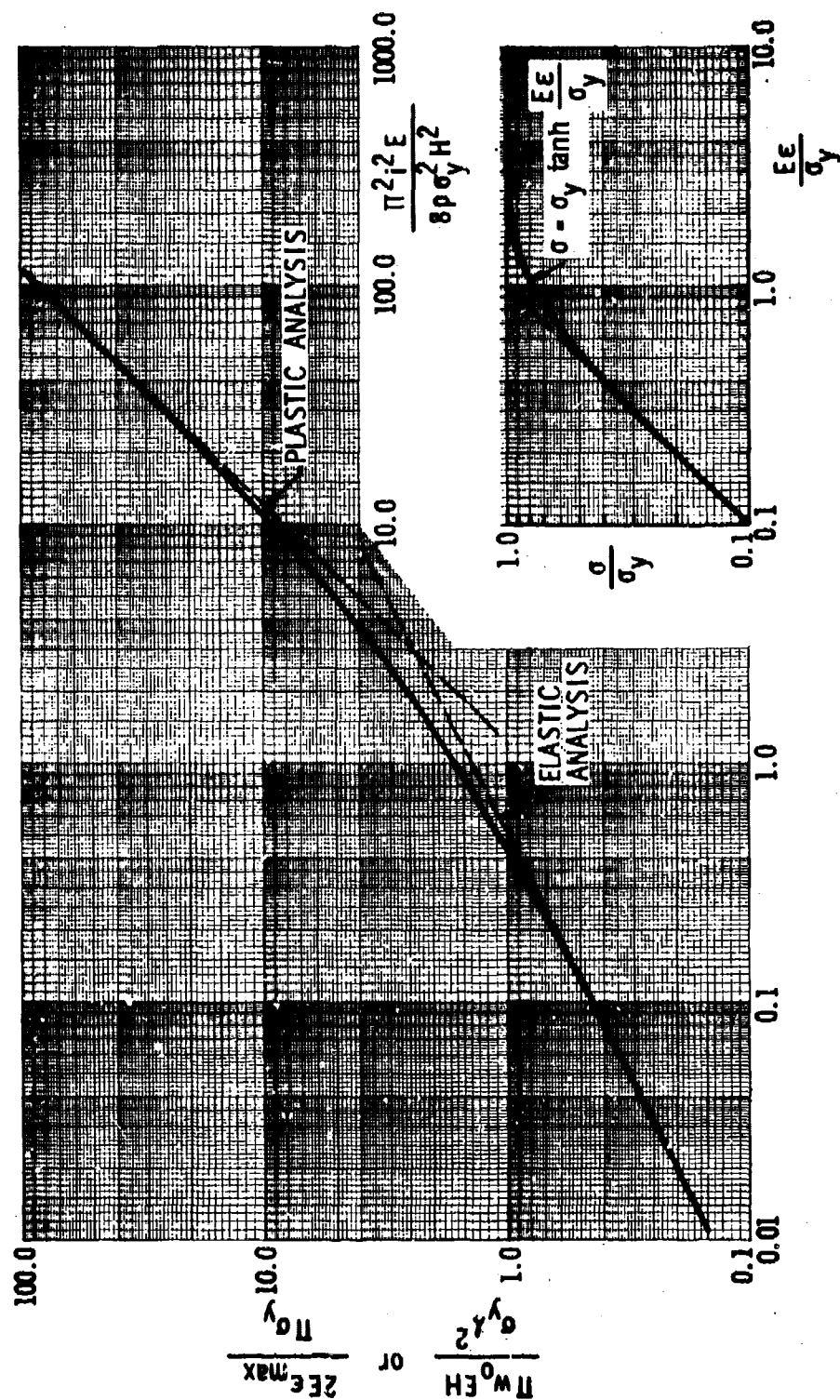
FIGURE 2. ELASTIC-PLASTIC SOLUTION FOR A SIMPLY SUPPORTED BEAM SUBJECTED TO A UNIFORM IMPULSIVE LOADING

33

The volume for an extensional element equals

$$\text{Vol.} = 2A \int_0^{\ell/2} dx \tag{98}$$

where A is the cross-sectional area.

Substituting Eqs. (97) and (98) into Eq. (89) gives the following integral equation for the strain energy U.

$$U = \frac{2\sigma_y^2 A}{E} \int_0^{\ell/2} \ell n \cosh\left[\left(\frac{\pi^2 w_0^2 E}{2\ell^2 \sigma_y}\right) \cos^2\left(\frac{\pi x}{\ell}\right)\right] dx \tag{99}$$

or, using Eq. (93b),

$$U = \frac{2\sigma_y^2 A \ell}{\pi E} \int_0^{\pi/2} \ell n \cosh\left[\left(\frac{\pi^2 w_0^2 E}{2\ell^2 \sigma_y}\right) \cos^2 \alpha\right] d\alpha \tag{100}$$

The kinetic energy imparted to a string equals:

$$KE = \frac{I^2}{2m} = \frac{i^2 b^2 \ell}{2\rho A} \tag{101}$$

Equating the kinetic energy to the strain energy and rearranging yields the nondimensional equation:

$$\left(\frac{\pi i^2 b^2 E}{4\rho \sigma_y^2 A^2}\right) = \int_0^{\pi/2} \ell n \cosh\left[\left(\frac{\pi^2 w_0^2 E}{2\ell^2 \sigma_y}\right) \cos^2 \alpha\right] d\alpha \tag{102}$$

This equation can be written as:

$$F = \int_0^{\pi/2} \ell n \cosh\left[G \cos^2 \alpha\right] d\alpha \tag{103a}$$

where

$$F = (\pi i^2 b^2 E / 4\rho \sigma_y^2 A^2) \text{ and } G = (\pi^2 w_0^2 E / 2\ell^2 \sigma_y) \tag{103b}$$

Numerical integration of Eq. (103) yields the solid line in Figure 3. As for the beam solution, the dashed lines in Figure 3 represent the asymptotes for fully elastic or fully plastic behavior, and the inset is a nondimensional plot of Eq. (86).

34
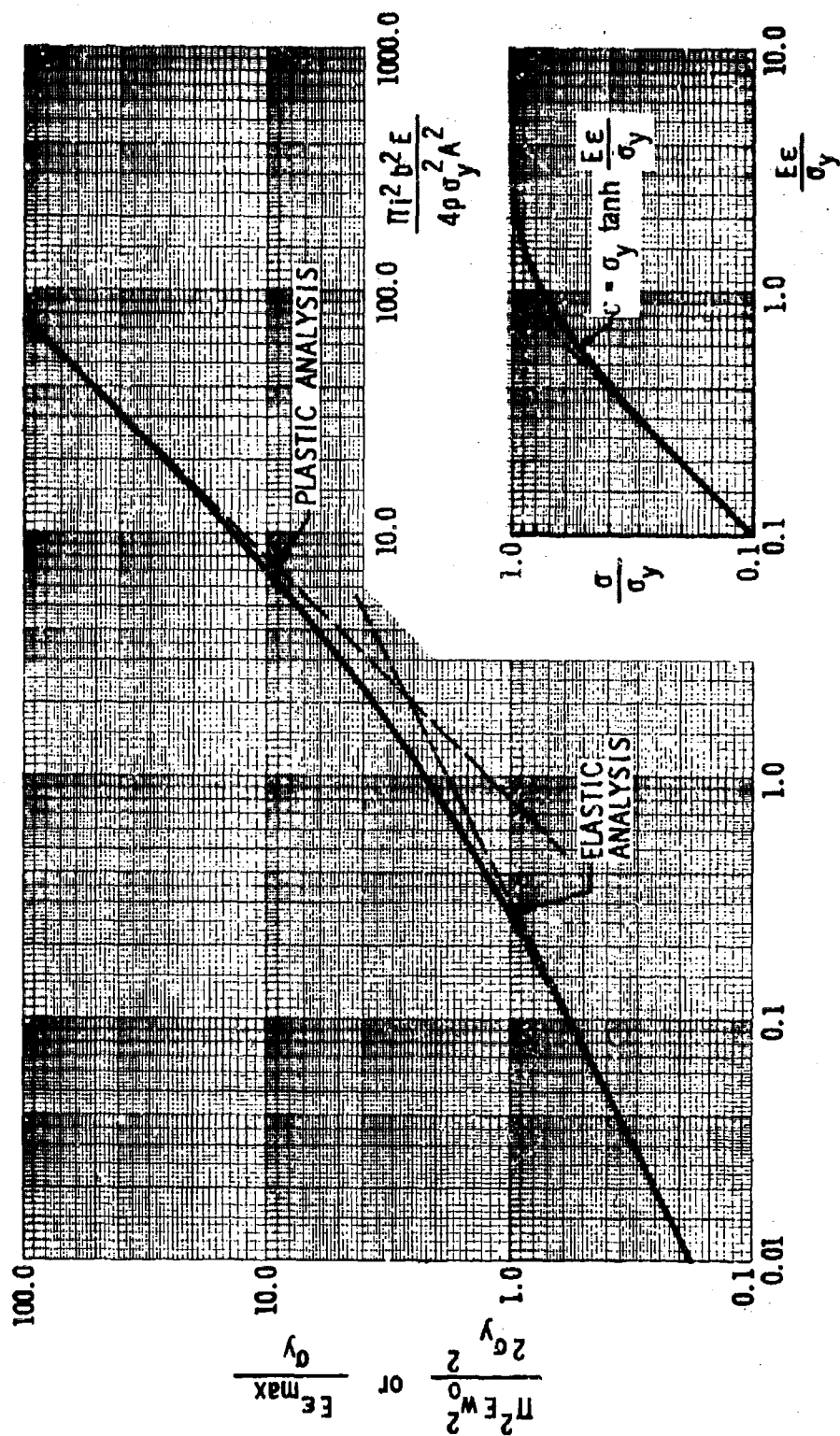
FIGURE 3. ELASTIC-PLASTIC SOLUTION FOR A STRING LOADED BY A UNIFORM IMPULSE

35

Although the elastic-plastic solutions given in Figures 2 and 3 are extremely useful for designers, they are somewhat difficult to derive because numerical integration is required. We will now show that the numerical solution can be approximated to within one or two percent by properly combining the elastic and plastic asymptotes. The asymptotes are easily derived.

3. Limiting Elastic and Plastic Cases

Before an approximate elastic-plastic solution can be found, the asymptotes are required. Although these limiting cases have been derived many times before (see Refs. 1, 4, 6, and 9), we will rederive them here for completeness.

In elastic problems, the strain energy per unit volume, Eq. (87) becomes:

$$\frac{U}{\text{Vol.}} = \frac{E}{2}\,\epsilon^2 \tag{104}$$

In plastic problems, the strain energy per unit volume, Eq. (87) becomes:

$$\frac{U}{\text{Vol.}} = \sigma_y \epsilon \tag{105}$$

Of course, these equations apply to either the beam or string solution.

For the beam solution, both elastic and plastic strains are given by Eq. (90), and the volume equals the double integral given by Eq. (91). Substituting these two equations into Eq. (104) for the elastic case or Eq. (105) for the plastic case gives:

elastic:

$$U = \frac{2\pi^4 E w_o{}^2 b}{\ell^4} \int_0^{H/2} \int_0^{\ell/2} h^2 \sin^2\left(\frac{\pi x}{\ell}\right)\, dh\, dx \tag{106}$$

rigid-plastic:

$$U = \frac{4\pi^2 \sigma_y w_o b}{\ell^2} \int_0^{H/2} \int_0^{\ell/2} h \sin\left(\frac{\pi x}{\ell}\right)\, dh\, dx \tag{107}$$

Or, after completing the required double integrations:

elastic:

$$U = \frac{\pi^4 E w_o{}^2 b H^3}{48\ell^3} \tag{108}$$

rigid-plastic:

$$U' = \frac{\pi \sigma_y w_o b H^2}{2\ell} \tag{109}$$

Now, by equating Eq. (108) to Eq. (94) and Eq. (109) to Eq. (94), the elastic and plastic asymptotes, respectively, of Figure 2 are obtained. These are given by Eqs. (110) and (111).

(elastic beam)

$$\frac{\dot{t}^2 \ell^4}{\rho E w_o^2 H^4} = \frac{\pi^4}{24} \tag{110}$$

and

(rigid-plastic beam)

$$\frac{\dot{t}^2 \ell^2}{\rho \sigma_y w_o H^2} = \pi \tag{111}$$

For the string solution, both elastic and plastic strains are given by Eq. (97), and the volume is given by the integral in Eq. (98). Substituting these two equations into Eq. (104) for the elastic string or Eq. (105) for the plastic string gives:

elastic:

$$U = \frac{\pi^4 E w_o^4 A}{4\ell^4} \int_0^{\ell/2} \cos^4 \left(\frac{\pi x}{\ell}\right) dx \tag{112}$$

rigid-plastic:

$$U = \frac{\pi^2 \sigma_y w_o^2 A}{\ell^2} \int_0^{\ell/2} \cos^2 \left(\frac{\pi x}{\ell}\right) dx \tag{113}$$

Or, after completing the required integrations:

elastic:

$$U = \frac{3\pi^4 E A w_o^4}{64 \ell^3} \tag{114}$$

37

rigid-plastic:

$$U = \frac{\pi^2 \sigma_y A w_o^2}{4\ell} \tag{115}$$

The elastic and plastic asymptotes for the string solution are obtained by equating Eqs. (114) and (115), respectively, to the kinetic energy given by Eq. (101). Equations (116) and (117) obtained in this way are the asymptotes of Figure 3.

(elastic string)

$$\frac{i^2 b^2 \ell^4}{\rho E A^2 w_o^4} = \frac{3\pi^4}{32} \tag{116}$$

and

(rigid-plastic string)

$$\frac{i^2 b^2 \ell^2}{\rho \sigma_y A^2 w_o^2} = \frac{\pi^2}{2} \tag{117}$$

The approximate elastic-plastic solutions can now be derived.

4. Approximate Elastic-Plastic Solutions

The elastic-plastic solutions in Figures 2 and 3 are very closely approximated by Eq. (118) where Y is the ordinate, X is the abscissa, and coefficients A and B are constants.

$$Y = A \tanh^2 (BX)^{1/2} \tag{118}$$

The elastic asymptote for Eq. (118) is:

(elastic asymptote)

$$\frac{Y}{X} = (AB) \tag{119a}$$

And the plastic asymptote is:

(plastic asymptote)

$$Y = (A) \tag{119b}$$

These equations have the same form as the asymptotes for the beam and the string. Thus, for the simply supported beam the terms in Eqs. (119) are defined by comparison with Eqs. (110) and (111). We find:

38

$$Y = \frac{l^2 \ell^2}{\rho \sigma_y w_o H^2} \qquad (120a)$$

$$\frac{Y}{X} = \frac{l^2 \ell^4}{\rho E w_o^2 H^4} \qquad (120b)$$

$$A = \pi \qquad (120c)$$

$$AB = \frac{\pi^4}{24} \qquad (120d)$$

Solving for X and B and substituting into Eq. (118) gives an accurate approximation to the elastic-plastic bending solution without encountering the inconvenience of a numerical integration of a complicated function.

$$\frac{l^2 \ell^2}{\rho \sigma_y w_o H^3} = 3.1416 \tanh^2 \left[1.1366 \left(\frac{E H w_o}{\sigma_y \ell^2} \right)^{1/2} \right] \qquad (121)$$

To compare with Figure 2, this solution can be recast in the format:

$$\left[\frac{\pi^2 l^2 E}{8 \sigma_y^2 H^2} \right] = 1.234 \left[\frac{\pi E w_o H}{\sigma_y \ell^2} \right] \tanh^2 \left[0.641 \left(\frac{\pi E w_o H}{\sigma_y \ell^2} \right)^{1/2} \right] \qquad (122a)$$

or

$$C = 1.234 \, D \tanh^2 (0.641 \, D^{1/2}) \qquad (122b)$$

Either of the preceeding formats is acceptable for the elastic-plastic beam solution. The advantage to the format given by Eq. (122) is that the deformation w_o is isolated on one side rather than appearing on both sides. Designers would prefer to isolate w_o in this manner because this deformation also directly determines the maximum strain. Equation (122) is *not* the computed line appearing in Figure 2; however, it is very difficult to detect differences in Eq. (122) and the computer solution.

Equation (118) and its asymptotes can also be used to obtain an accurate approximation to the string solution. The elastic and plastic string solutions are given by Eqs. (116) and (117). Comparing Eqs. (119) to these equations, we have:

$$\frac{Y}{X} = \frac{l^2 b^2 \ell^2}{\rho E A^2 w_o^4} \qquad (123a)$$

$$Y = \frac{l^2 b^2 \ell^2}{\rho \sigma_y A^2 w_o^2} \qquad (123b)$$

$$AB = \frac{3\pi^4}{32} \qquad (123c)$$

39

$$A = \frac{\pi^2}{2} \qquad \text{(123d)}$$

Solving for B and X and substituting into Eq. (118) yields:

$$\frac{l^2 b^2 \ell^2}{\rho \sigma_y A^2 w_o^2} = \frac{\pi^2}{2} \, \tanh^2 \left[2.356 \left(\frac{E w_o^2}{\sigma_y \ell^2} \right)^{1/2} \right] \qquad \text{(124)}$$

Or after modifying the format to isolate terms containing w_o on one side and using Eq. (103b),

$$\left[\frac{\pi i^2 E b^2}{4 \rho \sigma_y^2 A^2} \right] = 0.7854 \left[\frac{\pi^2 E w_o^2}{2 \sigma_y \ell^2} \right] \tanh^2 \left[0.6124 \left(\frac{\pi^2 E w_o^2}{2 \sigma_y \ell^2} \right)^{1/2} \right] \qquad \text{(125a)}$$

or

$$F = 0.7854 \, G \, \tanh^2 (0.6124 \, G^{1/2}) \qquad \text{(125b)}$$

This solution also approximates the more detailed elastic-plastic solution with the same degree of accuracy as the bending beam analysis. Philosophically, one should not be disturbed by the use of the hyperbolic tangent squared as a function for combining elastic and plastic solutions. After all, any solution requires an approximate stress-strain curve. No approximation to a stress-strain curve uniformly matches all materials. Instead of approximating the stress-strain curve, one can elect to approximate the strain energy transition from elastic to plastic as we have done.

D. Graphical Solutions for Beams

The procedures developed in the preceding section can be used to derive general graphical solutions for blast loaded structural elements. These graphs are attractive because they permit rapid solutions to difficult problems without recourse to complicated mathematical procedures. In fact, as we will demonstrate, the graphical solutions are self-contained and can be easily applied.

Our example for these solutions will be beams loaded in the same manner as those in the case of the Category I shield. These beams are subjected to an initial impulse produced by the shock wave, plus a long duration quasi-static pressure produced principally by the heating of air in a confined space. Because the blast wave part of the loading is described only by an initial impulse (not a pressure and impulse or pressure and time), this solution is suitable only when the duration of the overpressure in the blast wave is less than one-quarter of the fundamental period of the beams. The pressure, p, in this solution refers to the quasi-static pressure, *not* the blast wave overpressure.

In response to these loads, the beams undergo elastic and plastic deformations. For this example, coupling between the beams and rings is neglected, but different end conditions, i.e., simply-supported, clamped or a combination of the two, are included.

The solution to this problem is similar to the impulsively-loaded beam solved in Section C except that an additional term is required to define the energy produced by the action of the quasi-static pressure, p, on the beam as it displaces. With the addition of this term called the work, WK, the energy balance is written as

$$KE + WK = U \tag{126}$$

KE is the kinetic energy produced by the initial impulse, and U is the strain energy (elastic and plastic) stored or absorbed by the beam.

Kinetic energy is the same for each beam regardless of the support condition and is given by Eq. (94), derived previously. The work and kinetic energy depend upon the mode shapes assumed, and this will differ for each support condition. For these calculations, we have assumed that the deformed shape under dynamic loading is the same as the static deformed shape. The calculations are illustrated in detail for a simply-supported beam.

The static deformed shape for a uniformly-loaded, simply-supported beam is given by Eq. (127)

$$y = \frac{16w_o}{5\ell^4}(x^4 - 2\ell x^3 + \ell^3 x) \tag{127}$$

where w_o is the center deflection ($x = \ell/2$). We can now derive the work from the quasi-static pressure p as

$$WK = \int_0^\ell pby \, dx \tag{128}$$

where b is the beam loaded width and ℓ is its length. Substituting Eq. (127) into (128) and performing the required integration, the work is found to be

$$WK = \frac{16}{25} pb\ell w_o \tag{129}$$

As shown in Eq. (90), the strain in a beam cross-section at a distance h above or below the neutral axis is

$$\epsilon = -h \frac{d^2 y}{dx^2} \tag{130}$$

Again using the deformed shape of Eq. (127), we have

$$\epsilon = -h \frac{16w_o}{5\ell^4}(12x^2 - 12\ell x) \tag{131}$$

41

The strain energy can now be computed from Eq. (89); however, the solution can be made more general if we reformulate the strain energy in terms of gross cross section properties of the beam. This can be done by replacing the stress-strain constitutive relationship given in Eq. (86) by an approximation for the moment-curvature relationship. Such a relationship is given by Eq. (132)

$$M = M_p \tanh \frac{EIy''}{M_p}$$
(132)

where y'' is the second derivative of the beam displacement with respect to x (curvature), and M_p is the fully plastic moment of the beams. Notice that Eq. (132) has exactly the form of Eq. (82). It was not derived from Eq. (82) and represents a slightly different approximation to the stress-strain behavior. In fact, the stress-strain behavior will differ slightly for beams of different cross-sections.

The strain energy per unit length for a beam in bending can be written as

$$\frac{U}{dx} = \int_0^{y''} M_p \tanh \left(\frac{EIy''}{M_p} \right) dy'' = \frac{M_p^2}{EI} \ell n \cosh \left(\frac{EIy''}{M_p} \right)$$
(133)

For the total strain energy, Eq. (133) is integrated over the beam length, ℓ, to obtain:

$$U = \frac{M_p^2}{EI} \int_0^{\ell} \ell n \cosh \left(\frac{EIy''}{M_p} \right) dx$$
(134)

Substituting for y'' from Eq. (127) gives

$$U = \frac{M_p^2}{EI} \int_0^{\ell} \ell n \cosh \left[\left(\frac{EIw_o}{M_p \ell^4} \right) \frac{192}{5} (x^2 - \ell x) \right] dx$$
(135)

It is convenient to nondimensionalize the integral by letting

$$\xi = \frac{x}{\ell}; \quad dx = \ell d\xi$$
(136)

With these substitutions we have

$$U = \frac{M_p^2 \ell}{EI} \int_0^1 \ell n \cosh \left[\left(\frac{EIw_o}{M_p \ell^2} \right) \frac{192}{5} (\xi^2 - \xi) \right] d\xi$$
(137)

42

Now substituting Eqs. (94), (129), and (137) into Eq. (126), we obtain Eq. (138), which relates the deformation of a simply-supported beam to its basic properties and the blast loading parameters:

$$\frac{i^2 b^2 \ell}{2\rho A} + \frac{16}{25} pb\ell w_o = \frac{M_p^2 \ell}{EI} \int_0 \ell n \cosh\left[\left(\frac{EIw_o}{M_p \ell^2}\right) \frac{192}{5} (\xi^2 - \xi)\right] d\xi \qquad (138)$$

Equation (138) is nondimensionalized by dividing each side by the coefficient of the integral, or:

$$\frac{i^2 b^2 EI}{2M_p^2 A} + \frac{16pbEIw_o}{25M_p^2} = \int_0^1 \ell n \cosh\left[\left(\frac{EIw_o}{M_p \ell^2}\right) \frac{192}{5} (\xi^2 - \xi)\right] d\xi \qquad (139)$$

In nondimensional pi terms, the equation is:

$$\pi_1 + \pi_2 = \int_0^1 \ell n \cosh\left[\pi_3 \left(\frac{192}{5}\right) (\xi^2 - \xi)\right] d\xi \qquad (140)$$

A more convenient relationship is obtained if w_o is eliminated from all but one group. This is accomplished by rewriting π_2 as the product of π_3 and a new group π_2'.

$$\pi_2 = \pi_2' \cdot \pi_3 = \left(\frac{16pb\ell^2}{25M_p}\right) \left(\frac{EIw_o}{M_p \ell^2}\right) \qquad (141)$$

Also, if one wishes to limit the maximum strain in the beam rather than the maximum deformation, w_o can be replaced by ϵ_{max} in π_3 using Eq. (131). For a simply-supported beam, ϵ_{max} occurs at $x = \ell/2$ and $h = H/2$. Thus,

$$\epsilon_{max} = \frac{24Hw_o}{5\ell^2} \qquad (142)$$

With this substitution, π_3 becomes

$$\pi_3 = \frac{5EI\epsilon_{max}}{24M_p H} \qquad (143)$$

Now Eq. (139) becomes:

$$\frac{1}{2}\left(\frac{ib\sqrt{EI}}{M_p\sqrt{\rho A}}\right)^2 + \left(\frac{Pb\ell^2}{\alpha_p M_p}\right) \left(\frac{EI\epsilon_{max}}{\alpha_c M_p H}\right) = \int_0^1 \ell n \cosh\left[\left(\frac{EI\epsilon_{max}}{\alpha_c M_p H}\right)\right.$$

$$\left. \times \left(\frac{192}{5}\right) (\xi^2 - \xi)\right] d\xi \qquad (144)$$

43

where the constants in π_2' and π_3 have been replaced by α_p and α_ϵ, respectively.

Similar equations can also be derived for clamped-clamped and clamped-simply-supported beams. If we again use the static deformed shape under uniform loading, the following equations are obtained.

Deformed Shape

$$c\text{-}c\text{:} \quad y = \frac{16w_o}{\ell^4}(x^4 - 2\ell x^3 + \ell^2 x^2)$$

$$c\text{-}ss\text{:} \quad y = \frac{7.7w_o}{\ell^4}(x^4 - \frac{3}{2}\ell x^3 + \frac{1}{2}\ell^3 x)$$

Strain Equation

$$c\text{-}c\text{:} \quad \epsilon = -h\frac{32w_o}{\ell^4}(6x^2 - 6\ell x + \ell^2)$$

$$c\text{-}ss\text{:} \quad \epsilon = -h\frac{7.7w_o}{\ell^4}(12x^2 - 9\ell x)$$

Maximum Strain

$$c\text{-}c\text{:} \quad \epsilon_{max} = \frac{16Hw_o}{\ell^2}$$

$$c\text{-}ss\text{:} \quad \epsilon_{max} = \frac{11.55Hw_o}{\ell^2}$$

The deformed shapes are substituted into Eq. (128) to compute the work, and the strain expressions are substituted into Eq. (134) to compute the strain energy. These expressions are then combined with the kinetic-energy [Eq. (94)] according to Eq. (126) to obtain expressions similar to Eq. (138). Performing the manipulations described for simply-supported beams and generalizing the results, an equation can be obtained which applies to all three boundary conditions. It is given by Eq. (145).

$$\frac{1}{2}\left(\frac{tb\sqrt{EI}}{M_p\sqrt{\rho A}}\right)^2 + \left(\frac{pb\ell^2}{\alpha_p M_p}\right)\left(\frac{EI\epsilon_{max}}{\alpha_\epsilon M_p H}\right) = \int_0^1 \ell n \cosh\left[\frac{EI\epsilon_{max}}{\alpha_\epsilon M_p H}\right.$$

$$\left. \times (C_1\xi^2 + C_2\xi + C_3)\right] d\xi \quad (145)$$

Note that the only difference between Eqs. (145) and (144) is in the description of the nondimensional deformed shape. The proper equation for each beam boundary condition is obtained by substitution of the appropriate constants as defined in Table III:

44

TABLE III. CONSTANTS FOR EQUATION (141)

	α_p	α_e	C_1	C_2	C_3
clamped (c-c)	1.875	16	192	−192	+32
clamped-simply supported (c-ss):	1.732	11.55	92.4	− 63.3	0
simply supported (ss-ss):	1.5625	4.8	38.4	− 38.4	0

Equation (145) was numerically integrated for each beam boundary condition to obtain the graphical solution of Figure 4. To better understand the information presented in the figure, rewrite Eq. (145) in the following form:

$$\frac{1}{2}\pi_1^2 + \pi_2'\pi_3 = I \tag{146}$$

where I is the value of the integral. Note that if the applied pressure, p, is zero, then the dimensionless group π_2' is zero, and Eq. (146) becomes

$$\frac{1}{2}\pi_1^2 = I \tag{147}$$

This equation yields the asymptote for impulsive loading, or

$$A_1 = \pi_1|_{p=0} = \sqrt{2I} \tag{148}$$

Likewise, for $I = 0$, $\pi_1 = 0$, and the asymptote for pressure loading becomes

$$A_2 = \pi_2'|_{I=0} = \frac{I}{\pi_3} \tag{149}$$

Equation (146) can be written in terms of these asymptotes if it is multiplied by $1/I$. This gives

$$\left(\frac{\pi_1}{\sqrt{2I}}\right)^2 + \frac{\pi_2'}{I/\pi_3} = 1 \tag{150a}$$

or

$$\left(\frac{\pi_1}{A_1}\right)^2 + \frac{\pi_2'}{A_2} = 1 \tag{150b}$$

or

$$\pi_1^2 + \pi_2' = 1 \tag{150c}$$

This is the general form plotted in Figure 4. Because the integral I depends upon π_3 and the beam boundary conditions, the asymptotes A_1 and A_2 are given in the inset as a function
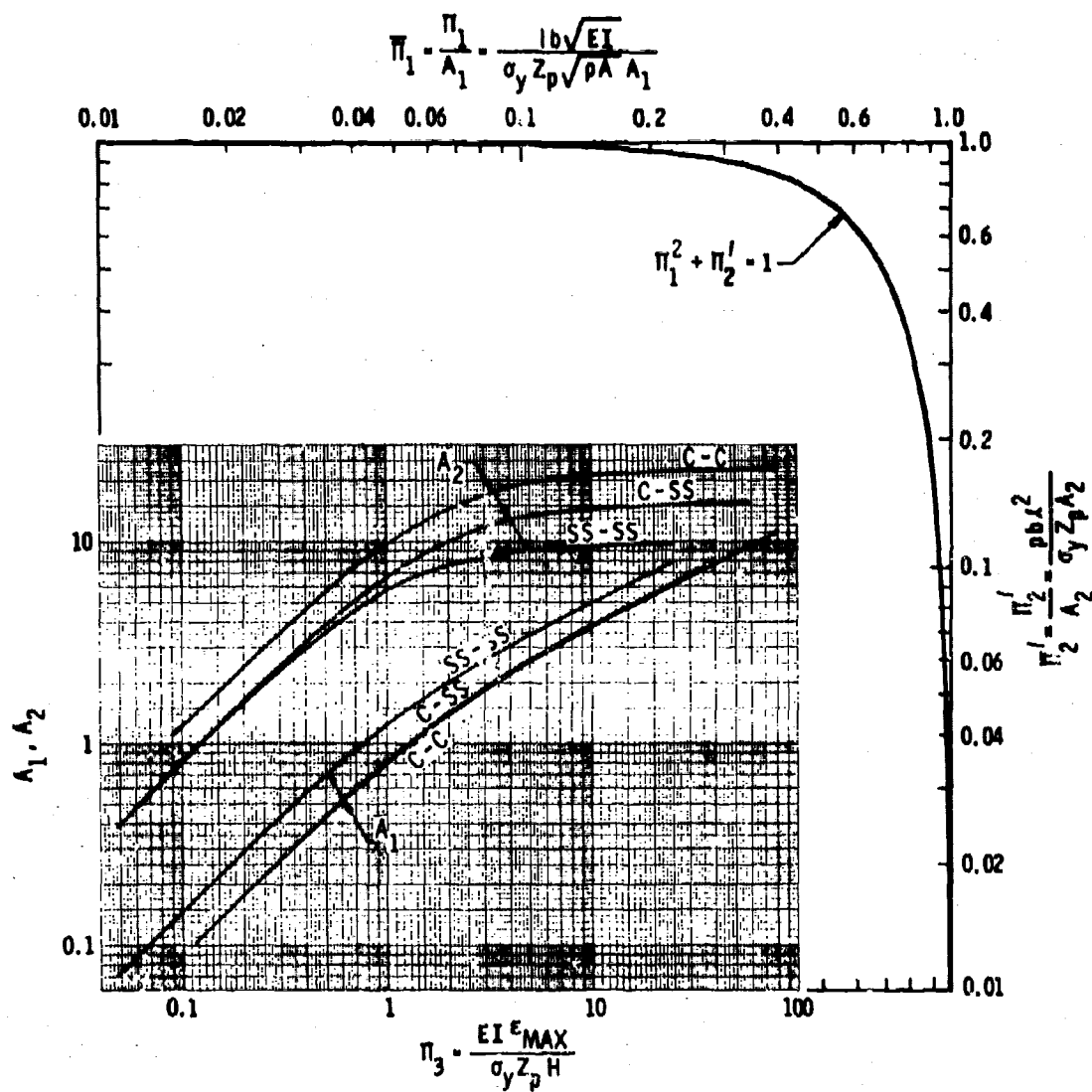
FIGURE 4. DESIGN CHART FOR ELASTIC-PLASTIC BEAMS SUBJECTED TO
INITIAL IMPULSE PLUS A QUASI-STATIC PRESSURE

46

of π_3 and the beam boundary conditions. One difference in the graphical solution and the form given by Eq. (145) is the absence of the constants α_p and α_e. Because separate curves are plotted for the different boundary conditions, these constants could be eliminated. For example, to eliminate α_p, the π_2' asymptote, A_2, was simply multiplied by the constant given for α_p in Table III for the appropriate boundary condition.

Observe that the solution for either impulsive loading only or for pressure loading only is given directly. This is clear from Eq. (150b) and from Figure 4. If $p = 0$, for example, then $\pi_3 = 0$ and we have

$$A_1 = \pi_1 = \frac{ib\sqrt{ET}}{\sigma_y z_p \sqrt{\rho A}} \tag{151}$$

Thus, if the beam properties and the impulse are known, A_1 can be computed and π_3 read directly from the appropriate curve in Figure 4. Alternately, if one wished to know what impulse would produce a prescribed strain in a beam, π_3 could be evaluated, A_1 read from the graph, and i computed from Eq. (151).

A similar approach holds for pressure loading only; however, for the case of an initial impulse plus a quasi-static pressure, an iterative approach is required. Consider as an example the beams in the cage of the Category 1 1/4-scale model. Beam properties and the loading parameters are listed below. (Refer also to Chapter IV.)

Beam Properties: Loading:

$A = 1.67$ in.^{2} $i = 0.48$ psi-sec
$I = 2.52$ in.^{4} $p = 190$ psi
$z_p = 1.95$ in.^{3}
$b = 1.43$ in. (loaded width)
$H = 3.0$ in.
$\ell = 30$ in.
$\sigma_y = 45,000$ psi
$E = 30 \times 10^6$ psi
$\rho = 0.000733$ lb-sec^2/in.^{4}

With these values, π_1 and π_2' can be computed.

$$\pi_1 = \frac{ib\sqrt{ET}}{\sigma_y z_p \sqrt{\rho A}} = 1.944$$

$$\pi_2' = \frac{pb\ell^2}{\sigma_y z_p} = 2.787$$

To find the maximum strain in the beams, first compute the values for pressure and impulse separately.

Impulse only: $A_1 = \pi_1 = 1.944$

47

From Figure 4 for a clamped (c-c) beam:

$$\pi_3 = \frac{EI\epsilon_{max}}{\sigma_y z_p H} \approx 3.2$$

$$\epsilon_{max} = 0.01114$$

Pressure only: $A_2 = \pi_2' = 2.787$

From Figure 4,

$$\pi_3 = \frac{EI\epsilon_{max}}{\sigma_y z_p H} \approx 0.235$$

$$\epsilon_{max} = 0.000818$$

The beam is more sensitive to the impulse than the pressure. Also, the maximum strain for the combined loading will be larger than the sum of the strains computed separately. Therefore, try

$$\epsilon_{max} = 1.1(0.01114 + 0.000818) = 0.01196$$

For this strain, π_3 is:

$$\pi_3 = 3.434$$

and from Figure 4,

$$A_1 = 2.02 \qquad A_2 = 17.9$$

A_1 and A_2 must satisfy Eq. (150b) (or the curve in Figure 4), which for this problem becomes

$$\left(\frac{1.944}{A_1}\right)^2 + \left(\frac{2.787}{A_2}\right) = 1$$

Substituting A_1 and A_2 gives

$$\left(\frac{1.944}{2.02}\right)^2 + \left(\frac{2.787}{17.9}\right) = 1.082$$

For a closer result, try

$$A_1 = 0.995 \frac{1.944}{\sqrt{1.0 - \frac{2.787}{17.9}}} = 2.1$$

From Figure 4, the corresponding values of A_2 and π_3 are

$$A_2 = 18.1$$

$$\pi_3 = 3.65$$

Now check Eq. (150b) again.

$$\left(\frac{1.944}{2.1}\right)^2 + \frac{2.787}{18.1} = 1.01 \approx 1$$

This result is close enough. Therefore, the maximum strain for the S3 × 5.7 beams in the Category I 1/4-scale model for clamped ends and rigid support is predicted to be

$$\epsilon_{max} = 3.65 \cdot \frac{\sigma_y z_p H}{EI} = 0.01271 = 12,710\mu\epsilon$$

Also note that, with the asymptotes A_1 and A_2 determined, the entire p-i diagram, for a maximum strain of $12,710\mu\epsilon$ in the beam, can be established from Eq. (150b) or from Figure 4. So, what we have really obtained is a general solution for the beam and not just the solution for one set of loading parameters.

If one wishes to compute maximum deflection in the beams, the relationship between maximum strain and the deflection can be used. For a simply-supported beam, this relationship is given by Eq. (142), and, for the other boundary conditions, by the expressions on page 44. Generalizing, we can write

$$w_o = \frac{\ell^2 \epsilon_{max}}{\alpha_\epsilon H} \tag{152}$$

where α_ϵ is given in Table III.

Thus, we have obtained a general graphical solution which includes:

● beams of different boundary conditions (with rigid support)
● elastic-plastic beam behavior
● predictions of maximum strains and deflections
● beam response predictions for any combination of an initial impulse, i, and quasi-static pressure, p.

Such a solution provides a convenient tool for preliminary design of beams subjected to this particular type of loading. For final design, a more rigorous approach is usually required, which includes the effects of support flexibility, etc. The need for a more rigorous analysis will be demonstrated by the comparisons in Chapter IV between measured and predicted strains for the Category I 1/4-scale model.

III. EQUATIONS FOR RESPONSE OF STRUCTURAL
ELEMENTS TO BLAST LOADING

Numerous equations for estimating the response of structural components to blast loading have been developed during the Suppressive Structures Program. Derivations of these equations have been reported by Baker, et al.,[1] by Westine and Baker,[6] and by Westine and Cox.[4] A partial summary was included in the report by Baker, et al.[9] Here, a final summary is made which collects the equations reported in References 1, 4, and 6, plus other equations that have not previously been reported. Equations presented are for the response of individual structural elements. Rigid behavior of the component which loads the element or the support for the element is assumed. Equations for coupled response have been developed for a few cases, but these are included separately in Chapter II. Chapter II also includes graphical solutions for selected components

This summary, given in Table IV, is an expansion of Table B-1 in Reference 9. Corrections to equations have been made, as required, and both elastic, elastic-plastic and rigid-plastic solutions are included. Structural elements covered include beams, rings, membranes, plates, cylinders, and spheres.

Equations in Table IV relate the peak deformation in the structural element, usually designated as w_o, to the element's material and geometric properties and to the applied loading. The applied loading is treated as the simultaneous application of an impulse, i_r, and a quasi-static pressure, p. This loading is representative of that on suppressive structures produced by the internal detonation of a high explosive. The blast wave from the detonation is of short duration relative to structural frequencies (and so can be treated as an impulse), and heating of the air in the structure produces a pressure buildup of much longer duration. Simultaneous application of the impulse and quasi-static pressure is supported by pressure measurement from the 1/16-scale venting tests reported by Schumacher and Ewing[11] and by pressure data from the Category 1 1/4-scale model tests reported by Schumacher, et al.[12] For purposes of deriving the equations, the quasi-static pressure is assumed to be a step loading (zero rise time) to a constant value. If either i_r or p is zero, the equations reduce to the proper pressure or impulsive asymptote, respectively.

Each equation is based upon an assumed shape for the final deformed state of the structural elements. The deformation patterns used are given in the table. For some elements, solutions are given for more than one deformed shape. This is true for a beam with clamped ends which experiences bending deformations only. The first solution used a parabola as the deformed shape, and the second solution uses a higher order polynomial. Deformations predicted by the first equation compare favorably to experiment[1]; however, bending strains in the beam associated with a parabolic deformed shape are constant. The second equation has not been compared to experiment, but the strain distributions produced by the deformed shapes are more representative of true beam behavior. A third solution is also given which is based upon the static deformed shape. Notice that the constants in the equations derived for the polynomial and for the static deformed shape differ only slightly.

Parameters which enter the equations in Table IV are defined in Table V. Also, the geometry of the element is sketched in Table IV for additional clarification. Because the equations are nondimensional in their present form, any consistent set of units is permissible.

TABLE IV. SUMMARY OF ENERGY SOLUTIONS FOR ESTIMATING THE DEFORMATION OF
STRUCTURAL ELEMENTS SUBJECTED TO UNIFORM BLAST LOADING

Structural Element	Geometry	Deformed Shape	Strain Energy	Response Formula for Outboard Lateral Deflection and Second-Order Pressure

Cantilever beam

Simply-supported beam, bending only

Clamped beam, bending only

51

TABLE IV. SUMMARY OF ENERGY SOLUTIONS FOR ESTIMATING THE DEFORMATION OF STRUCTURAL ELEMENTS SUBJECTED TO UNIFORM BLAST LOADING (Cont'd)

Structural Element	Geometry	Deformed Shape	Strain Behavior	Response Formula for Combined Initial Impulse and Quasi-Static Pressure
Beam bending, membrane and strain hardening B = 1, simply supported B = 2, clamped		$w = w_0\left(1 - \frac{4x^2}{L^2}\right)$	E-P	
Clamped-fixed beam, bending only			E-P	
Clamped rectangular plate, bending and membrane shear			E-P	
Clamped circular plate, bending and membrane action		$w = w_0\left(1 - \frac{r}{a}\right)$	E-P	
Simply-supported circular plate, bending only		$w = w_0 \cos\frac{\pi r}{2a}$	E-P	
Thin wall cylinder, no end restraint		$\Delta R = \text{constant}$	E	
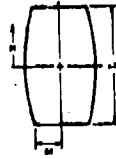
Structural Element	Geometry	Deformed Shape	Strain Behavior	Response Formula for Combined Initial Impulse and Quasi-Static Pressure
Thin wall cylinder, with end restraint, stretching mode only		$\Delta R \sim \Delta R_0 \left(1 - \dfrac{4x^2}{L^2}\right)$	E-P	$\dfrac{\pi x_0^2}{4 \rho h\, C_y} = \left(1 - \dfrac{\Delta R}{C_y R}\right)\dfrac{\Delta R}{R} + 4\dfrac{E}{L}\,\dfrac{\xi^2}{L}\left(\dfrac{\Delta R}{R}\right)^2$
Ring supporting rigid beams, cylinder configuration		$\Delta R = \text{constant}$	E	$\dfrac{2v_0^2 z_1^2 z_2^2}{C_y^2 R^2 R} = \dfrac{\Delta R}{R} - \dfrac{\sigma_y}{E}\left(\dfrac{\Delta R}{R} - \dfrac{2\sigma_y z_1 z_2}{E R_0}\right)$
			E-P $\left(\dfrac{\Delta R}{R} > \dfrac{\sigma_y}{E}\right)$	$\dfrac{2v_0^2 z_1^2 z_2^2}{C_y^2 R^2 R} + \dfrac{\sigma_y}{E} = \tau\,\dfrac{\Delta R}{R}\left(1 - \dfrac{\sigma_y z_1}{C_y R}\right)$
Sphere or dome without base restraint		$\Delta R = \text{constant}$	E	$\dfrac{\xi^2}{2t\left(\frac{L}{1-\nu}\right)(\Delta h + \sigma_y)} = \dfrac{\Delta R}{R} \cdot \dfrac{\sigma_y}{E} - \dfrac{\sigma_y}{\left(1-\nu\right)E}$
			E-P $\left(\dfrac{\Delta R}{R} > \dfrac{(1-\nu)\sigma_y}{E}\right)$	$\dfrac{\xi^2}{2\rho h(\Delta h + \sigma_y)} + \dfrac{(1-\nu)\sigma_y}{E} = \dfrac{\Delta R}{R}\left(2 - \dfrac{R_y}{C_y}\right)$

TABLE V. DEFINITION OF SYMBOLS USED IN TABLE IV

Symbol	Definition
A	beam cross-sectional area
A_R	ring cross-sectional area
b	loaded width of beam
CSB_R	circumferential beam spacing in the I-beam cylinder measured at R_R
E	material elastic modulus
h	thickness of plate, or shell
i_r	specific reflected impulse from initial blast wave, plus reflections if applicable
L	length of beam for which the deformation is being determined; length of cylinder
L_l	loaded length of the cylinder supported by a single ring
m_a	mass per unit area of any additional material (non load bearing) which is attached to the sphere or dome
M_T	total mass supported by a ring (includes the ring mass)
M_P	beam plastic moment
N	factor in the beam equation; $N = 1$ for simple support, $N = 2$ for clamped support
p	quasi-static pressure
P_y	axial yield force of the beam
r	radius to arbitrary point on a circular plate
R	mean radius of a sphere or cylinder, radius of a circular plate
R_L	loaded radius in the cylindrical shield
R_R	mean radius of the ring
ΔR	radial expansion of the ring, dome, or cylinder
w	lateral deflection of a beam or plate at point x, or r, respectively
w_o	center deflection of a beam or plate
x	distance along the beam or plate, normally measured from the center
X	short semi-span of the plate
y	distance along plate center line normally measured from the plate center
Y	long semi-span of the plate
ρ	material density
σ_y	yield strength of the material
ν	Poisson's ratio

IV. CATEGORY I 1/4-SCALE STRAIN DATA ANALYSIS

Measurements of strain in the beams, rings, foundation, and roof of the Category I 1/4-scale model were made by Schumacher, et al.,[12] in tests conducted at the BRL. Model dimensions and strain gage locations are shown in Figures 5 and 6. Structural details are given in the Corps of Engineers' drawing No. 6003, "Suppressive Shield, Quarter Scale Model, Category I." One of the principal objectives of the tests was to determine the structural adequacy of the shield and to evaluate the analytical methods used to support the shield design.

SwRI was assigned the task of analyzing strain data recorded on the beams and rings. Data were provided by BRL in the form of computer-generated plots. The plots were reviewed and peak strains were extracted from records which appeared to be consistent from test to test and with gages at similar locations. These peak values were then compared with analytical predictions. The comparisons allowed us to draw some conclusions about the strains and analysis methods which are covered at the end of this chapter.

A. Review and Summary of Experimental Data

A brief description of each test conducted on the model is given below. All charges were spherical Pentolite, centrally located. Closure strips and liners referred to in the test descriptions are shown in Figure 5.

Test 191: 8.3-lb charge—1/4-scale model without closure strips or liner

Test 192: Same as Test 191, but with a charge of 19.3 lb

Test 193: 19.3-lb charge—closure strips added to cover the spaces between every second pair of inside beams

Test 194: 19.3-lb charge—all spaces between the inside beams covered with closure strips

Test 195: 45.7-lb charge—same configuration as for Test 194 except that additional weld bead was added along the sides of the closure strips, and shims were added to eliminate free travel by the beam before contact with the ring was made.

Test 196: 45.7-lb charge—weld repairs were made and a 24-gage corrugated steel liner was added inside the closure strips to seal the shield.

Test 197: 45.1-lb charge—ring repairs were made, and two 22-gage corrugated steel liners were added inside the closure strips to seal the shield.

We limited our comparisons between analysis and experiment to those tests with all closure strips installed. Thus, comparisons were made with data from Tests 194 through 197 and include comparisons for both the 19.3-lb and 45.7-lb charge weights.

Figures 7 and 8 are typical of the strain plots received from BRL. Bending strains at the base of column 112 (see Figure 6) are given in Figure 7 for Test 192 and Tests 194
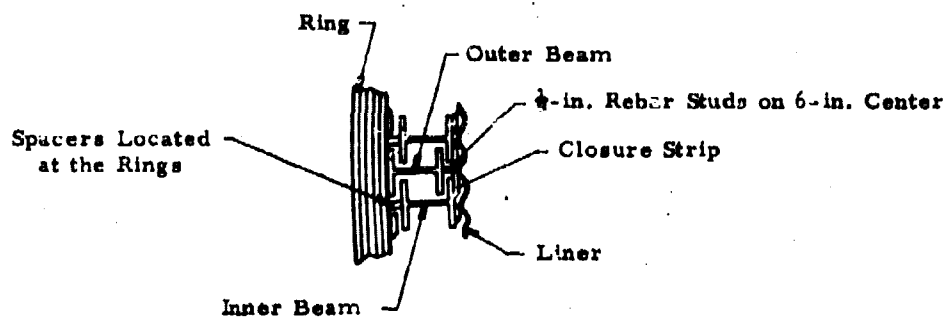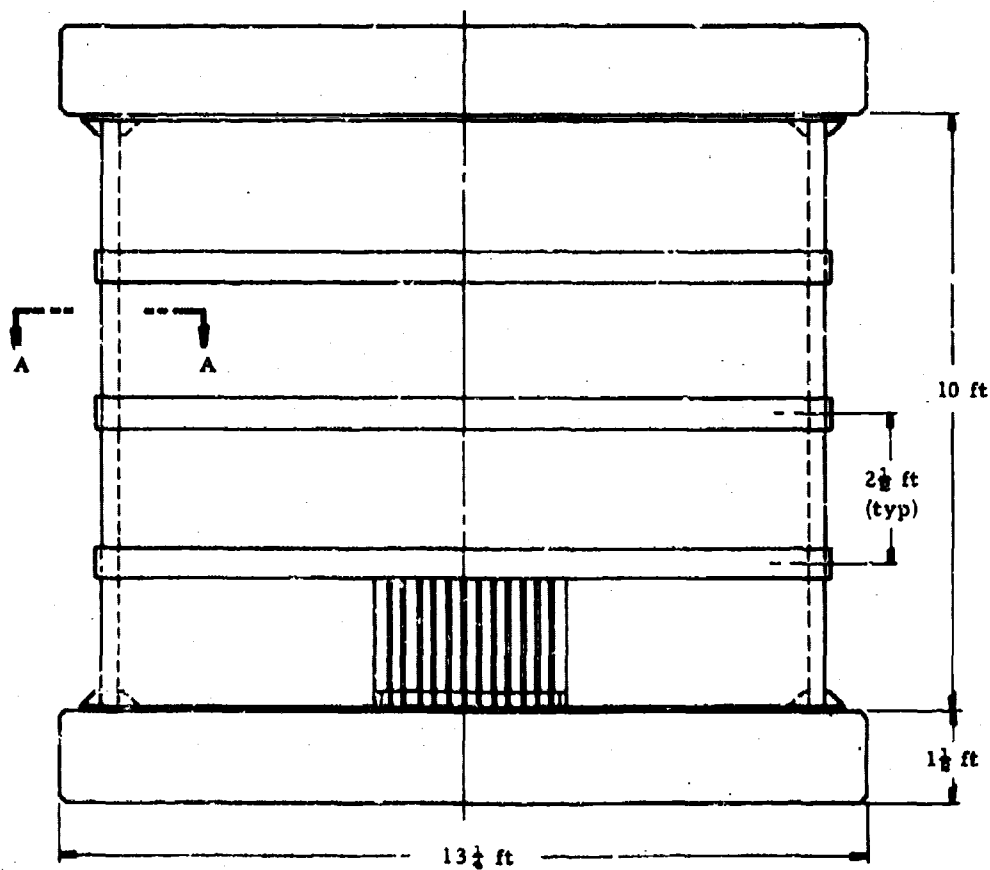
FIGURE 5. DIMENSIONS AND DETAILS OF THE
CATEGORY I 1/4-SCALE MODEL

Location	Gage Nos.			
	0°	90°	180°	270°
Upper Band	90	95	91	94
Middle Band	92	96	93	97
Lower Band	Not instrumented			
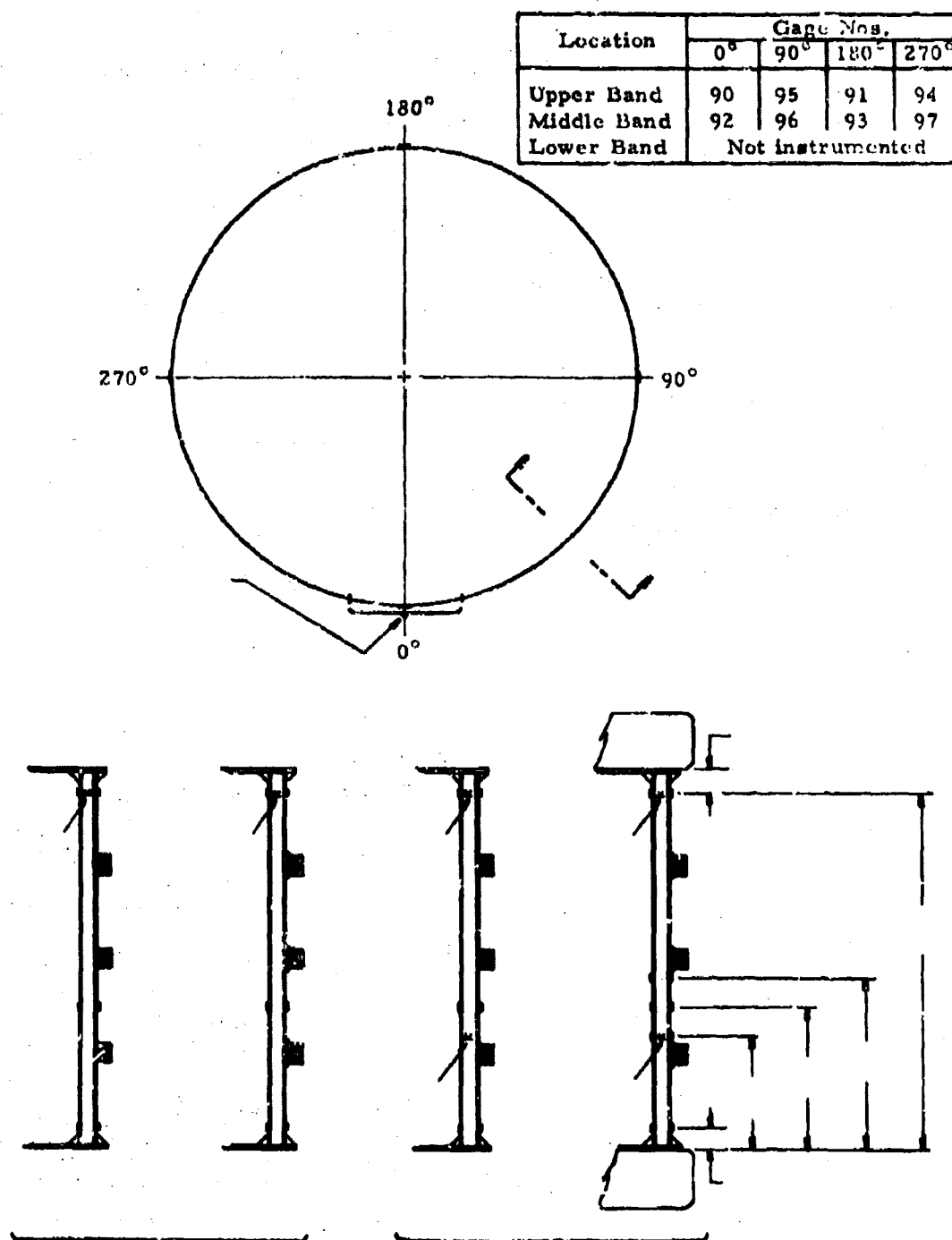
FIGURE 6. STRAIN GAGE LOCATIONS ON THE BEAMS AND RINGS

57
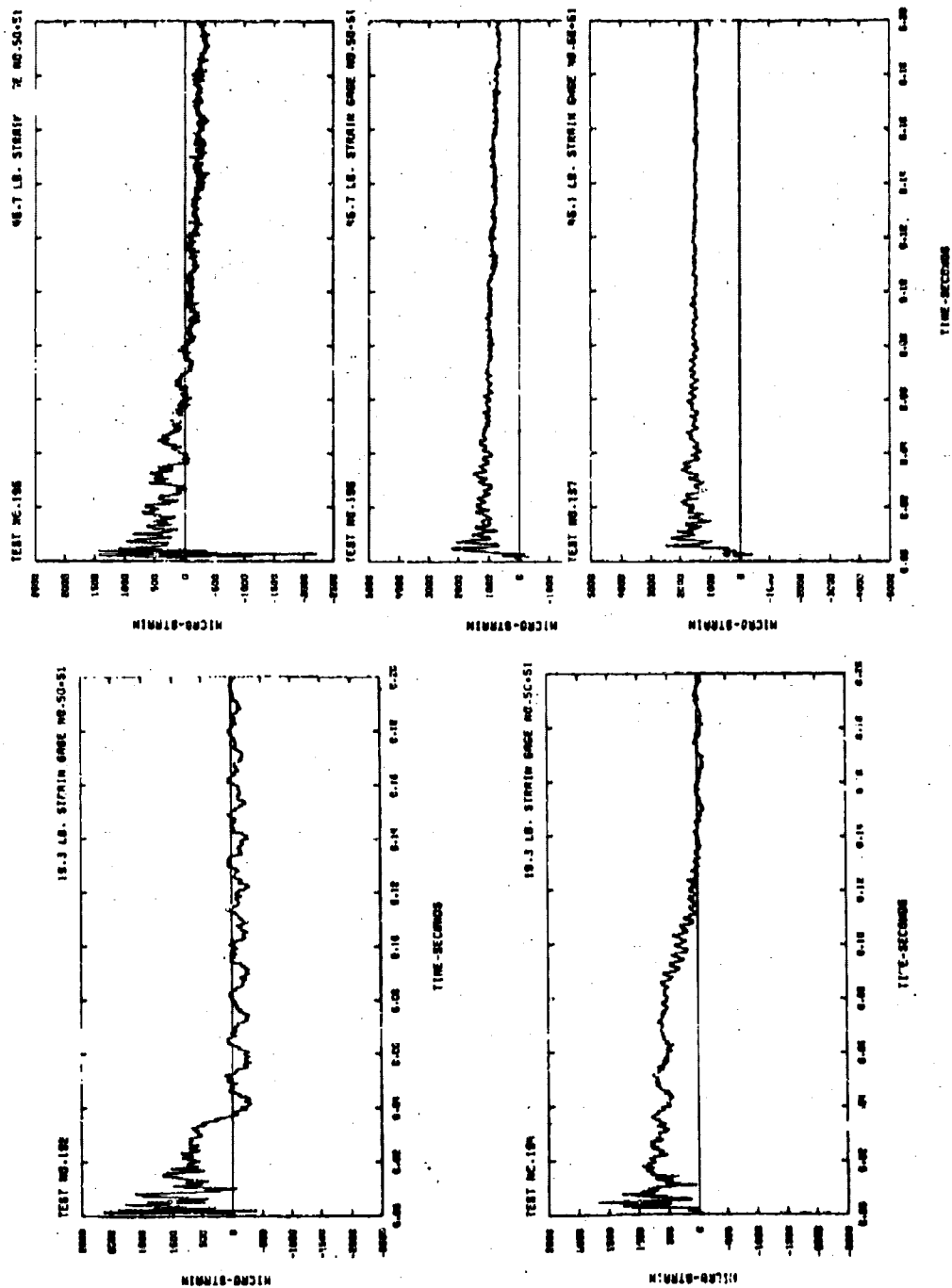
FIGURE 7. BENDING STRAINS MEASURED AT THE BASE OF COLUMN 112
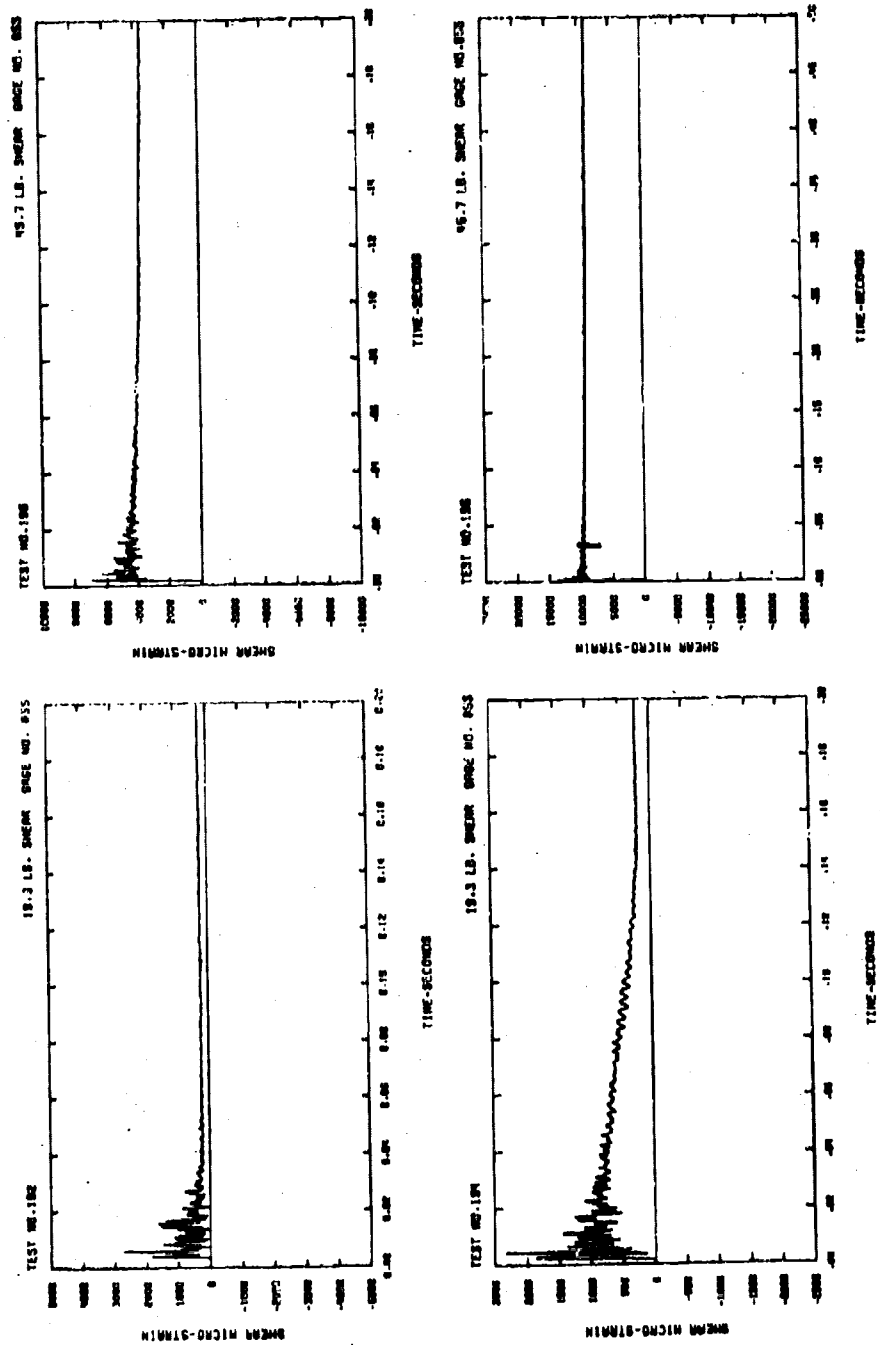
FIGURE 8. SHEARING STRAINS MEASURED AT THE TOP OF COLUMN 259

through 197. The effect of progressive sealing of the shield is apparent from the reduced decay rates. The character of Test 195 is noticeably different from the others because it decays sooner than expected and has a negative value late in time. Shims were inserted between the beams and the rings before this test, and the change in response character can be attributed to the change in support. Figure 8 gives the history of the principal strain computed from rosette No. 85, which is located at the top of column 259. From these records it appears that slight yielding in shear occurred even in the early tests. Reasons for the pronounced increase in shearing strain between Tests 195 and 196 are not clear. Again, it may have been caused by firmer beam support after the beams were shimmed against the rings. The principal shearing strain for Test 197 (not shown) may have been caused by firmer beam support after the beams were shimmed against the rings. The principal shearing strain for Test 197 (not shown) was slightly higher than for Test 196. A more detailed interpretation of the strain records is given by Schumacher, et al.[12]

Peak strains read from the graphs of Figures 7 and 8 and from other graphs provided by BRL are listed in Tables VI, VII, and VIII. Table VI contains the bending strains reduced from gage pairs on the inside and outside flanges of the beams. Location of the gages above the top surface of the foundation is included in the table, and the placement of the gages on the beam is shown in Figure 6. Principal shearing strains in the beams are given in Table VII and peak tensile strains in the rings are given in Table VIII. In all cases, the strain data for Test 191 (the 8.3-lb test) and for Test 193 (the 19.3-lb test with only half of the closure strips installed) have been omitted. Test 192 was included to indicate the effect which the closure strips have on the peak strains. No consistent difference is apparent in the beam strains. Ring strains are increased slightly.

TABLE VI. MAXIMUM BENDING STRAINS* OBTAINED FROM BRL RECORDS
OF CATEGORY I 1/4-SCALE MODEL TESTS

Location† (in.)	Gage Nos.	19.3-lb Charge		45.7-lb Charge		
		Test 192	Test 194	Test 195	Test 196	Test 197
6-3/8	50-51	1050	840	700	1100	1250
	56-57	1175	1200	–	875	–
	66-67	–	–	–	–	–
	72-73	–	–	–	–	–
34-1/2	58-59	−975	−1000	−1450	–	–
45	60-61	−1850	–	–	–	–
	74-75	–	−1350	−1165	–	−1600
	68-69	–	–	–	–	–
55-1/2	62-63	−1000	−1000	−900	–	−1450
113-5/8	54-55	1300	1225	1090	1155	1135
	64-65	1100	1240	–	1150‡	–
	70-71	–	–	–	–	–
	76-77	1350	1450	–	1150	–

*Strains are in μin/in.; (+) represents tension on inside edge of the beam.
†Measured from top of floor slab (see Figure 6).
‡Estimated from one gage only.

60

TABLE VII. MAXIMUM SHEAR STRAIN* OBTAINED FROM BRL RECORDS
OF CATEGORY 1 1/4-SCALE MODEL TESTS

Location† (in.)	Rosette No.	19.3-lb Charge		45.7-lb Charge		
		Test 192	Test 194	Test 195	Test 196	Test 197
34-1/2	78	1700	2650	3250	--	--
	81	--	--	--	--	--
113-5/8	80	....	--	--	--	--
	83	2150	2000	2500	7500	--
	84	--	1550	2400	--	--
	85	2800	2350	7000	14000	14810

*Strains are in µin/in.
†Measured from top of floor slab (see Figure 6).

TABLE VIII. MAXIMUM RING STRAINS* OBTAINED FROM BRL RECORDS
OF CATEGORY I 1/4-SCALE MODEL TESTS

Location†	Gage No.	19.3-lb Charge		45.7-lb Charge		
		Test 192	Test 194	Test 195	Test 196	Test 197
Top Ring	90	--	1060	2580	2400	2200
	91	−1430	--	3100	2400	4200
Middle	92	1450	1600	--	3300	3400
Ring	93	1150	2300	2800	2100	3100

*Strains are in µin/in.
†See Figure 6.

B   Comparisons with Analytical Predictions

For comparison with the measured strains of Tables VI, VII, and VIII, strains in the beams and rings were computed using both the approximate energy procedures described in Section II and finite-element methods. Application of the energy methods to compute structural response has been reported in References 1, 4, 7, 9, and 10, and in earlier chapters of this report, so these energy methods will be used here with a minimum of explanation. Application of the finite element program to compute structural response will be described more thoroughly.

1.   Predictions Using Approximate Energy Methods

a.   Uncoupled Solution

The blast loads associated with a confined explosion as in a suppressive structure are not the same as the blast loads associated with an unconfined explosion. Initially in a confined explosion, a shock wave is propagated out away from a source; however, because

61

of the walls in the container, this initial shock is reflected many times until through various dissipation mechanisms, the air is heated and a static pressure buildup of very long duration results. In the suppressive structures program, this multiple loading mechanism was mathematically modeled by treating the initial shock wave as a delta function (as an impulse) and the long duration buildup of internal pressure as a constant static pressure.

The generalized solution for the response of a beam in bending to this type of loading is given in Figure 4 of Chapter II. As in all solutions for structural elements, ideal boundary conditions are assumed, and coupling between the element and its supporting structure are neglected. For the Category I model, the assumption of clamped-clamped boundaries for the beams is most appropriate.

Beams in the model are S3 X 5.7. Properties of the beam cross-section are obtained from the Steel Construction Handbook and the remainder of the beam geometry from Figure 5. Loads on the beam are produced by the initial reflected blast wave and by the subsequent quasi-static pressure. Impulse in the blast wave is obtained from the data presented by Baker.[13] The quasi-static pressure is determined using the procedure developed by Baker, et al.[1] Compiling the input data for Figure 4 from the above sources, we have

Geometry:

$A = 1.67$ in.^{2} (area of the beam)

$b = 1.43$ in. (loaded width—less than flange width because of overlap)

$H = 3.0$ in. (beam depth)

$z = 1.95$ in.^{3} (beam plastic section modulus)

$I = 1.65$ in.^{4} (beam elastic section modulus)

$a_y = 45,000$ psi (material yield strength)

$E = 30 \times 10^6$ psi (elastic modulus)

$\rho = 7.33 \times 10^{-4}$ lb-sec^2/in.^{4} (material density)

Loading Parameters:

	19.3-lb Charge	45.7-lb Charge
Reflected impulse, $i_r =$	0.20 psi-sec	0.48 psi-sec
Quasi-static pressure, $p_{qs} =$	73 psi	190 psi

A yield strength greater than the minimum guaranteed for the material was chosen because limited measurement on structural steel conducted during the suppressive structures program showed yield values between 40,000 psi and 50,000 psi.

Maximum beam strain for the 45.7-lb charge weight was computed in Chapter II, Part D, as an example for the use of Figure 4. The calculated strains given in Table IX were obtained using the same procedure for the loading produced by the 19.3-lb charge.

62

Charge Weight (lb)	Calculated ($\mu\epsilon$)	Measured ($\mu\epsilon$)
19.3	3,730	1450
45.7	12,700	1600

For the 19.3-lb charge, data from Test 194 rather than Test 192 were used. The peak strain occurred at the top of an inside beam. For the 45.7-lb charge, the maximum measured strain was midway between two supports (two rings) on the same beam. The gages which recorded the maximum strain for the 19.3-lb charge were no longer operative for the tests with the 45.7-lb charge, so bending strains at the top of the beam might have been greater. Even if this were so, it is apparent that the predicted strains are much larger than measured values. This is particularly true for the 45.7-lb charge.

The predictions of Table IX were obtained by, in effect, treating the rings as rigid and absorbing all of the energy produced by the blast in the beams only. Obviously, these predictions are much too conservative to be of practical use in shield design. Similarly, ring response, computed for the assumption of rigid beams, is much too great. Thus, the energy absorbed must be properly divided between the beams and the rings, and this requires a coupled solution.

b. Coupled Solution

A solution for the coupled response of two structural components, one supported by the other, is described in Chapter II and Reference 10. It assumes rigid-plastic behavior with loads applied to the supported structure only. The loading is comprised of an initial impulse and a quasi-static pressure as for the uncoupled solution described previously. For beams supported by rings (hoops) as in the Category I shield, the response of the system is given by Eq. (64) of Chapter II. This equation, repeated here for convenience, gives the motion of the center of the beam, w_o, relative to the rings.

$$\frac{I^2 b^2 \ell^2}{\rho_b A_b \sigma_b z w_o} + \frac{p b \ell^2}{N \sigma_b z} \left[1.0 + \frac{N \rho_b A_b \ell}{4 \pi \rho_h A_h R} \frac{\left(\frac{2 N \sigma_b z}{\sigma_h A_h \ell} - 1 \right)}{\left(1 - \frac{p r \ell}{2 \sigma_h A_h} \right)} \right] = 8\pi + \frac{\sigma_h \rho_b A_b \ell^2}{\sigma_b \rho_h z R} \frac{\left(\frac{2 N \sigma_b z}{\sigma_h A_h \ell} - 1 \right)}{\left(1 - \frac{p r \ell}{2 \sigma_h A_h} \right)}$$

(64)

Once w_o is found, Eq. (59), also taken from Chapter II, gives the total radial motion, ΔR, of the ring in terms of w_o.

$$\frac{w_o}{\Delta R} \approx \frac{8\pi \left(\frac{\rho_h A_h R}{N \rho_b A_b \ell} \right) \left(1 - \frac{p_q r \ell}{2 \sigma_h A_h} \right)}{\left[\left(2 \frac{N \sigma_b z}{\sigma_h A_h \ell} \right) - 1 \right]}$$

(59)

63

Based on the maximum deflections, w_o and ΔR of the beam and ring respectively, the residual strains are computed from Eqs. (65a) and (65b).

$$\epsilon_r = \frac{\Delta R}{R} \qquad (65a)$$

$$\epsilon_b = \frac{\pi^2 w_o H}{\ell^2} \qquad (65b)$$

To compute residual strains in the Category I 1/4-scale model using these equations, the following parameters are required:

$\sigma_b = \sigma_h = 45{,}000$ psi (material yield strength)

$\rho_b = \rho_h = 7.33 \times 10^{-4}$ lb-sec^2/in.^{4} (material density)

$A_b = 1.67$ in.^{2} (beam cross-section area)

$z = 1.95$ in.^{3} (beam plastic section modulus)

$N = 296$ (no. of beams supported by the rings)

$b = 1.43$ in. (beam loaded width—less than flange width because of overlap)

$\ell = 30$ in. (beam length)

$H = 3.0$ in. (beam depth)

$A_h = 5.625$ in.^{2} (one-half of the ring area)

$R = 72.25$ in. (radius to center of the ring)

$r = 67.25$ in. (internal radius of the shield)

Blast loads are the same as listed on page 62.

Results obtained with the coupled solution are compared to the experiment in Table X. Both beam and ring strains are included. Calculated strains are residual, whereas the measured strains are peak. It is not appropriate to simply add the elastic strain at yield ($\epsilon_y = \sigma_y/E = 1550$ μin./in.) to the residual strain, but the peak strain would lie between the residual strain, ϵ_r, and the residual plus elastic strain ($\epsilon_r + \epsilon_c$). With this in mind, the agreement between the calculated and measured strains is good. Very little yielding, if any, occurred in the beams, and this is predicted by the analysis. Predicted ring strains are higher than measured for the 45.7-lb charge. One reason for this may be that the nine individual bands from which the ring was assembled were not in good contact. This means that higher strains occurred in the inner bands than in the outer bands where the measurements were made. Also, many rings broke near the welds, which may indicate an embrittlement problem.

64

TABLE X. COMPARISON OF BEAM AND RING STRAINS:
EXPERIMENT TO COUPLED ENERGY SOLUTIONS

Structural Component	19.3-lb Charge		45.7-lb Charge	
	Calculated Residual (μe)	Measured (μe)	Calculated Residual (μe)	Measured (μe)
Beams	200	1450	390	1600
Rings	975	2300	6,880	4200

As can be seen by comparing the results in Tables IX and X, the use of coupling is to greatly reduce the calculated estimates. Although the estimates are still not in perfect agreement, the coupled predictions are much closer to measured values than are the uncoupled predictions. Even better prediction should be achieved with finite element methods.

2. Predictions by Finite Element Methods

In addition to the energy solutions, a small two-dimensional (2-D) finite element computer program, developed specifically for the dynamic-transient analysis of beams to blast loading, was used to predict structural response of the Category 1 1/4-scale model. The equations of motion are cast in finite difference form and integrated step-wise in time using a predictor-corrector method. The program treats material behavior as bilinear with hysteretic recovery, including the effects of strain rate and strain hardening. Calculations of the response were made with and without strain rate to show the significant effect strain rate has on displacements and strains. Strain hardening effects were found to be negligible and are not discussed further.

The finite element model used for the calculations is shown in Figure 9. It is drawn schematically alongside one of the beams from the cylinder. The structure is idealized by assuming axial symmetry and symmetry about a horizontal plane through the center of the shield. This amounts to neglecting the presence of the door on the response of the beams away from its immediate vicinity, and neglecting axial loading and response. Although there is some connection between the beams through the closure strips, which are tack welded to the face of the inner beam and to the studs on the outer beam (see Figure 5), the beams are assumed to respond individually. Thus, only the lower half of one beam is represented in the model.

Bilinear springs have been used to model the rings and radial flexibility in the foundation. The resistance of the rings is divided into two parts to spread the support over the ring width. Guided end conditions permit lateral displacements, but no rotation, and the first beam element above the foundation has been sized to represent the combined bending stiffness of the slab foundation and the bolted connection. Although the closure strips may contribute to the beam stiffness, they are not welded continuously to the beams, and so this contribution is ignored; however, mass of the closure strips and the liners is added to the beam mass.

Center
Ring

Shield ℄

Lower
Ring

Z

R

Foundation

Guided End
Condition (typ)

Beam Element

Bi-linear
Spring

Lumped Mass
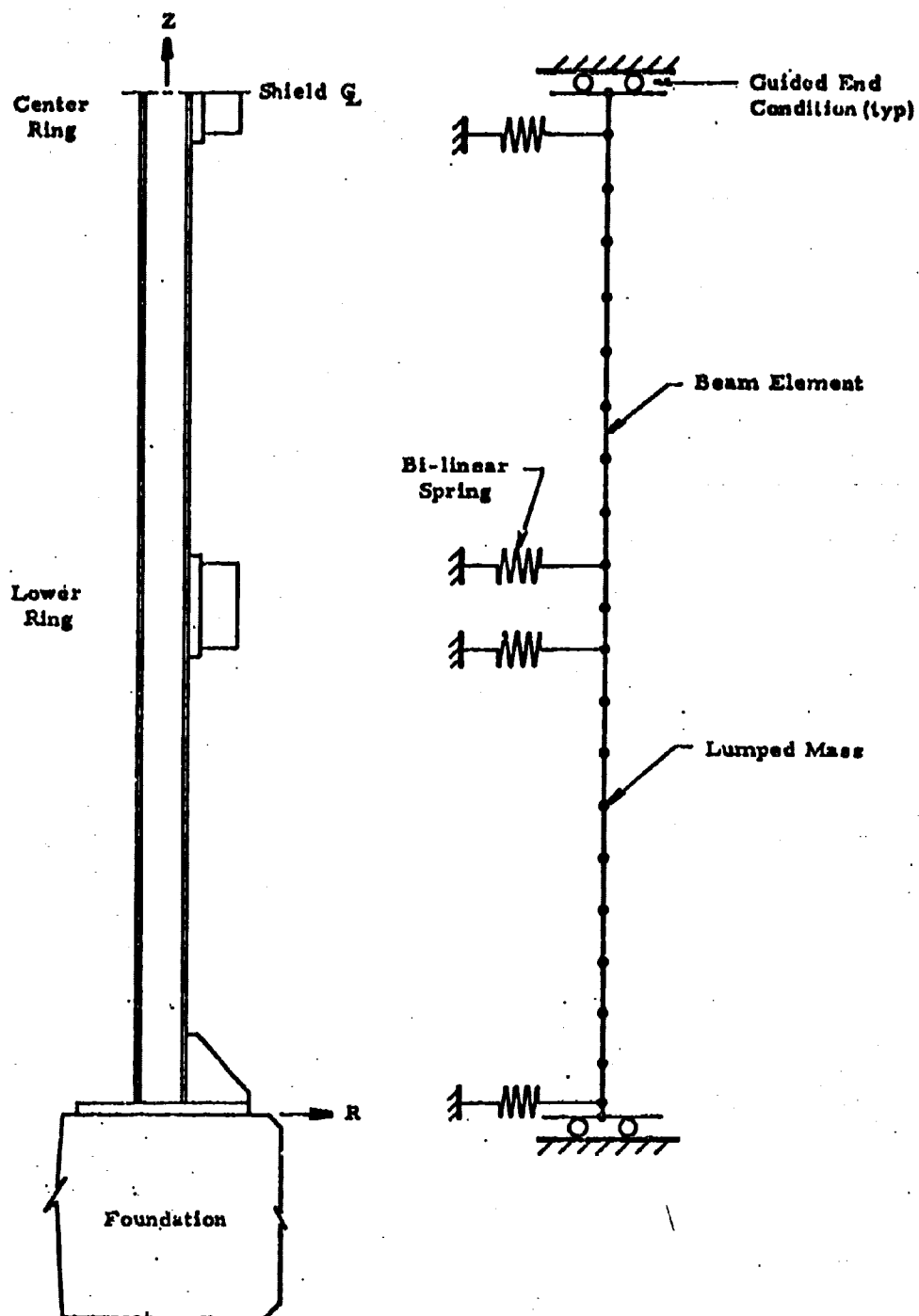
FIGURE 9. SCHEMATIC OF THE FINITE ELEMENT
MODEL OF THE STRUCTURE

66

As for the energy solutions, the pressure loading was assumed to be uniformly distributed over the beam. The loading is composed of an initial impulse and near constant (quasi-static) pressure. Two load cases were analyzed. They are the same as listed on page .

19.3-lb charge: i_r = 0.20 psi-sec

                      p_{qs} = 73 psi

45.7-lb charge: i_r = 0.48 psi-sec

                      p_{qs} = 190 psi

Basic beam and ring parameters used in computing input for the program are:

- S3 × 5.7 beam geometry

- mass per unit length (including closure strips and liners),
  $A = 1.46 \times 10^{-3}$ lb-sec/in.^{2}

- foundation effective modulus, $E_c = 4.5 \times 10^6$ psi

- beam plastic moment, $M_y = 87.750$ in./lb

- beam elastic modulus, $E = 29 \times 10^6$ psi

- beam plastic modulus = 1% of elastic modulus

- beam loaded width, $b = 1.43$ in.

Although the details will not be given, stiffness of the reinforcing gussets at the foundation and of the spacers at the rings was added to the beam. Also, estimates were made of the bending stiffness of the beam attachment to the foundation. Strain rate effects are based on the well known relationship[14] for mild steel given in Eq. (153)

$$\sigma_d = \sigma_y \left[1 + \left(\frac{\dot{\epsilon}}{40.4} \right)^{0.2} \right] \qquad (153)$$

where σ_d is the dynamic yield stress, and $\dot{\epsilon}$ is the strain rate.

Results for the 19.3-lb charge are given in Figure 10. Strain rate effects are included. This figure shows the distribution of maximum values of displacement, bending strain, and shear stress along the beam. The shear stress is based on the shear reactions in the beam rather than on shearing strains, and is computed as

$$\sigma_s = \frac{V}{d t_w} \qquad (154)$$

where V is the shear reaction in the beam, d is the beam depth, and t_w is the beam web thickness. Data points are shown as circles. Three observations can be made from this comparison:

(1)   The distribution of peak strains in the beam is irregular and not what one would expect if only a section of the beam between two rings were analyzed.

67
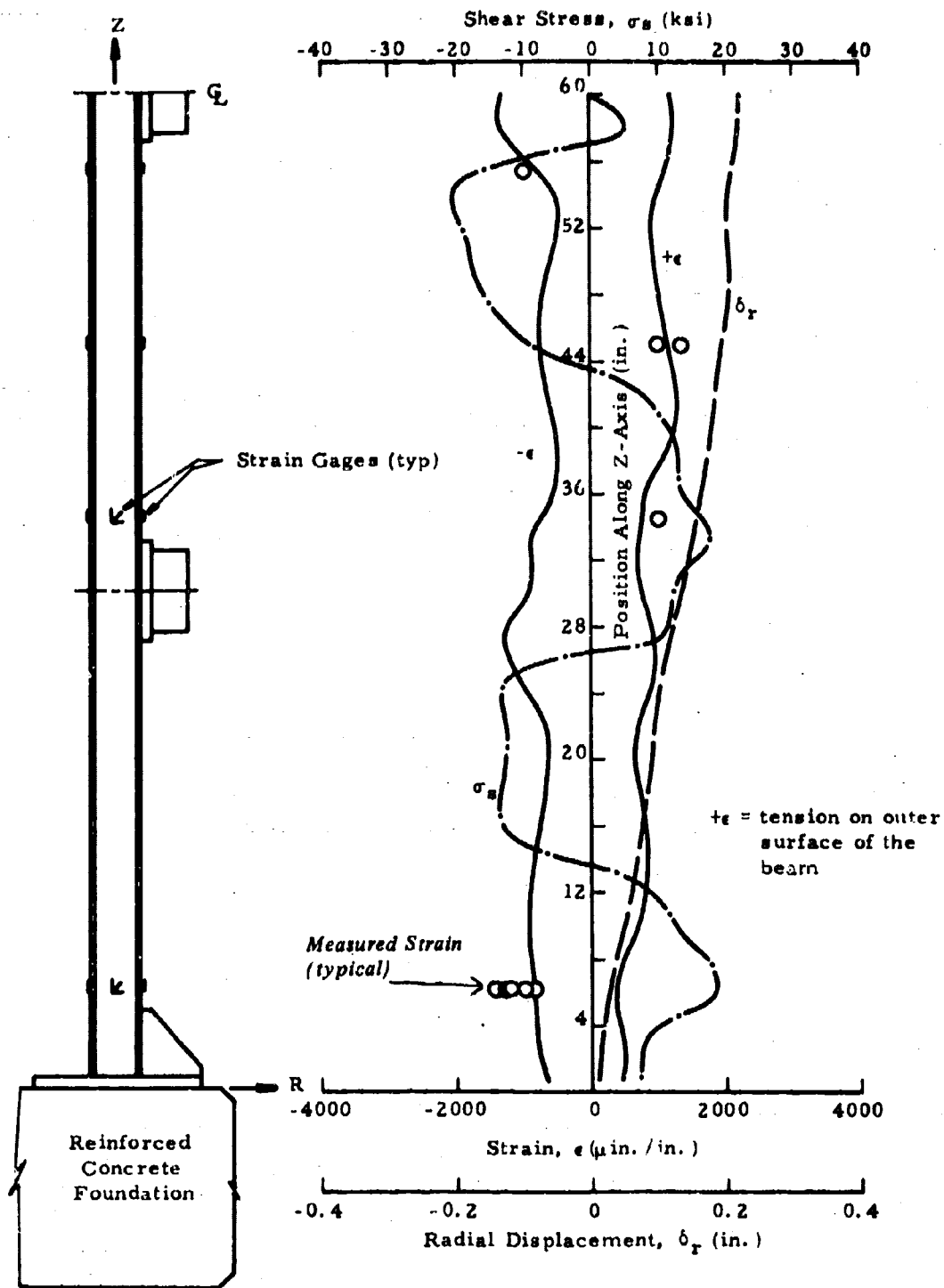
FIGURE 10. DISTRIBUTION OF MAXIMUM DEFLECTION, STRAIN
AND SHEAR STRESS VALUES (19.3 lb charge)

68

(2) Computed results for bending strains underestimate the measured values for this charge weight (at the measurement location).

(3) If the computed distribution of strain is accurate, the measurement point may not have recorded the maximum values.

Figure 11 gives similar results for the 45.7-lb charge. The same observations can be made for this case as were made for the smaller charge except that, in this instance, the computed strains are higher than measured values. Also, for this charge weight the shearing stresses exceed the shear yield stress of the material at many points along the beam. We estimate that the allowable shear stress values for the material are:

$$\sigma_{sy} = 21,600-27,000 \text{ psi}$$

$$\sigma_{su} = 34,800-49,800 \text{ psi}$$

These compare to peak calculated values of 44,000 psi, which indicates that substantial yielding of the beam in shear should have occurred, and perhaps the beam was near shear failure.

Although strain comparisons cannot be made because shearing strains were not computed by the program, Table XI lists measured shear strains versus the computed stress. The measured results confirm that substantial yielding occurred in shear for the 45.7-lb charge. Shear strains slightly beyond yield were also recorded for the 19.3-lb test. These results, plus the results in Figure 11, indicate that the beam is not properly proportioned for highly impulsive short duration loading. Higher shear area relative to bending stiffness is needed to bring the shearing and bending strains into better balance. This observation is true for almost all commercially available beams because they have been designed for high efficiency under static loads.

TABLE XI. BEAM SHEAR DATA

Location	19.3-lb		45.7-lb			Calc. Stress F.E. Prog
	Meas. Strain Test 194	Calc. Stress F.E. Prog	Measured Strain			
			Test 195	Test 196	Test 197	
Outer beam 34-1/2" from foundation	2,650*	18,000†	3,250	--	--	35,000
Outer beam 6-1/4" from roof	1,550	20,000	2,400	--	--	44,000
Inner beam 6-1/4" from roof	2,000	20,000	2,500	7,500	--	44,000
Inner beam 6-1/4" from roof	2,350	20,000	7,000	14,000	14,800	44,000

*Strain μ in./in.
†Stress psi.

69
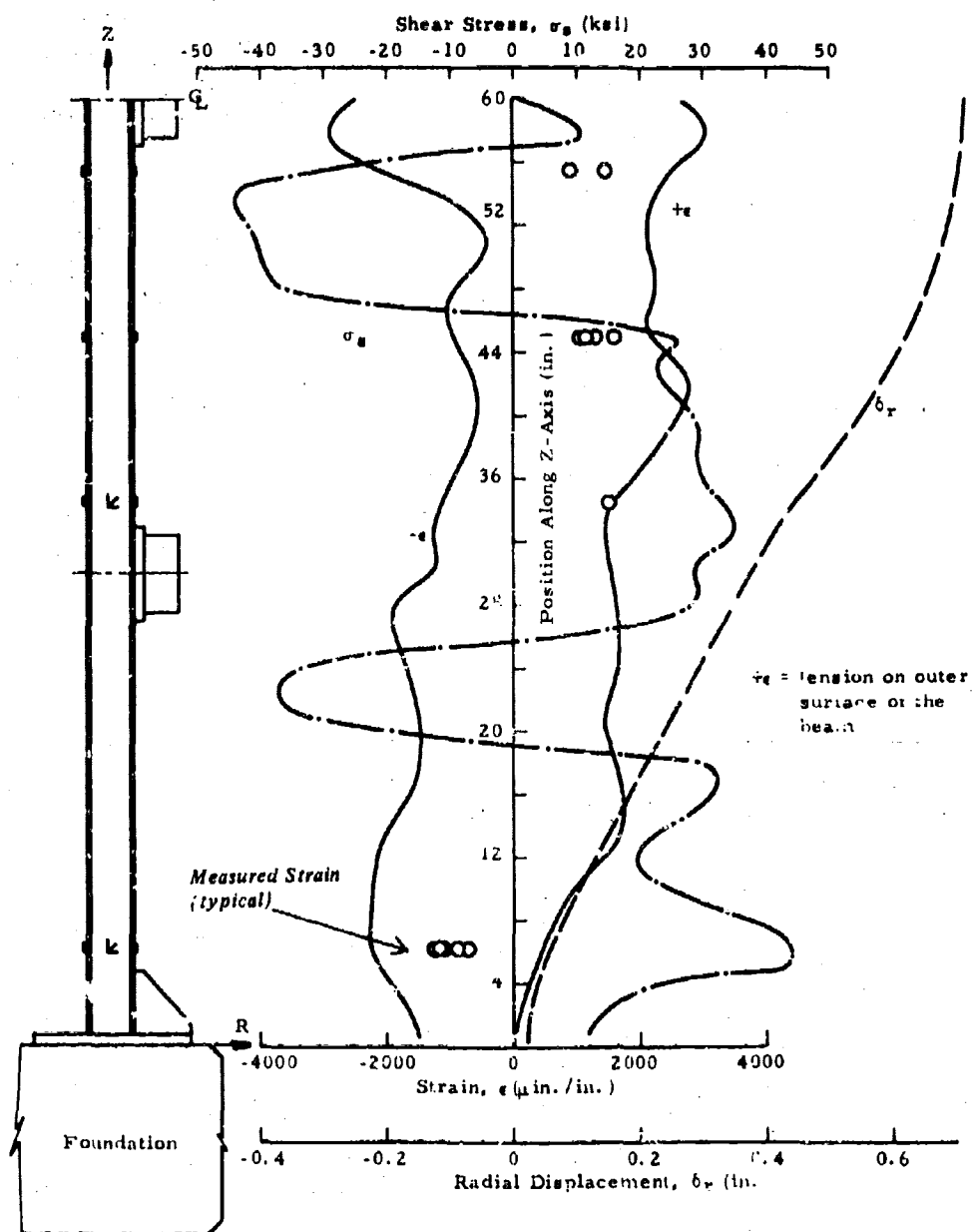
FIGURE 11. DISTRIBUTION OF MAXIMUM DEFLECTION, STRAIN
AND SHEAR STRESS VALUES (45.7 lb charge)

70

Only results which included strain rate effects were presented in Figures 10 and 11. The effects of strain rate on the overall structural response are best demonstrated by the variation in ring strains. Measured and calculated strains are given in Table XII. Calculated values include those obtained by energy formulas as well as by the finite element program. For the energy solutions, both coupled and uncoupled results are included. The coupled solution was obtained from Eqs. (59) and (64); the equation for uncoupled response is given in Table IV of Chapter III.

TABLE XII. MEASURED AND CALCULATED STRAINS IN THE RINGS

| | 19.3 lb | | 45.7 lb | |
	Test 194	Test 195	Test 196	Test 197
Top Ring				
Measured				
Gage 90*	1100†	2200	2400	2200
Gage 91	--	5100	2400	4200
F.E.‡ Solution				
No S.R.**	5315		13630	
With S.R.	1840		5110	
Energy Formulas				
No coupling	3100		18490	
With coupling	2460		6320	
Center Ring				
Measured				
Gage 92	1600	--	3300	3400
Gage 93	2300	--	2100	3100
F.E. Solution				
No S.R.	10360		21530	
With S.R.	3000		9740	
Energy Formulas				
No coupling	3100		18490	
With coupling	2490		6824	

*Refer to Figure 7 for gage locations.
†Strains are in μ in./in.
‡Finite element 2-D program.
**Strain rate effects.

The most obvious conclusion to be reached from the results in Table XII is that the calculated values overestimate measured ring response in every case. For the two comparisons available, it appears that the difference between computed and measured values increases as charge weight increases; hence, the analytical results should always be conservative. The effects of strain rate and coupling are pronounced, reducing calculated values by approximately a factor of three for the large charge weight. Still, the calculated values are far above measured values. It should be noted that the energy solution does not include strain rate or strain hardening effects and yet gives a result which is the same order of magnitude as the

71

more rigorous finite element method. One reason for this is that the energy solution forces plastic deformation in the beams, whereas the finite element solution does not. It is apparent from Figure 11 that predicted plastic straining in the beams was minimal so that energy absorption by the beams was small.

Reasons for the disagreement between predictions and measurements of ring response are not clear. However, two factors may have affected the results:

(1) The closure strips shown in Figure 5 were tack welded to the inner beams and provided some circumferential restraint. Thus, the closure strips acted in a manner similar to rings, but were distributed over the full height of the shield. This effect was neglected in the response calculations.

(2) Properties of the rings material were never measured. It proved to be a brittle material because fractures were noted during the testing. The calculations were performed assuming a mild steel, which may not represent true ring properties.

One final comparison of measured and calculated results is given in Table XIII. It compares peak measured strains in the beam to strains and shearing stresses computed by both the energy and finite element methods. From this comparison, it is obvious that both the finite element solution with strain rate effects and the coupled energy solution give results which are consistent with the measured values. Additionally, the finite element method provides useful information on shear in beams by providing shear reactions which predict the presence of large shearing strains. From the finite element solution, it is also apparent that strain rate effects play little part in the beam bending response. By stiffening the ring, however, strain rate does cause higher shear stresses. This stiffening of the ring was demonstrated in Table XII by the sharp reduction in the ring strain.

TABLE XIII. COMPARISON OF PEAK VALUES IN THE BEAMS

	19.3 lb charge			45.7 lb charge		
	Bending Strain μ in./in	Shear Strain μ in./in.	Shear Stress psi	Bending Strain μ in./in.	Shear Strain μ in./in.	Shear Stress psi
Measured	1450	2650		1600	14,800	
F.E. Method						
No SR	--		--	3010		36,900
With SR	1400		20,000	3000		44,000
Energy Solution						
Uncoupled	3730			12700		
Coupled (Residual)	200			390		

C. Conclusions from the Strain Data Analysis

The conclusions drawn from these comparisons of analysis and experiment are:

(1) Strain data, provided by BRL in the form of computer generated plots, appear to be good. The data are surprisingly consistent from test to test for a structure which was being altered continuously and undergoing plastic strains. Exceptions occur, and these can usually be explained by major alterations to the structure, such as shimming the beams prior to Test 195.

(2) Measured beam bending strains are lower than expected and did not increase significantly with an increase in charge weight.

(3) Shear strains in the beam web were high. Yielding occurred as predicted by high shear forces which were calculated for the beams.

(4) Ring strains were much lower than predicted, particularly for the large charge weight.

(5) The comparisons show that the energy solution for coupled response can give reasonable answers, which, if in error, tend to overestimate the strains.

(6) The finite element computer solutions show that strain rate should not be ignored in structural components which respond primarily in a stretching mode, such as for the rings. If these effects are ignored, the solution is an upper bound, but it is too conservative to be useful if reasonably accurate predictions are desired.

V. PRESSURES FROM BURNING PROPELLANT IN VENTED CHAMBERS

The thrust of this effort was to determine theoretically the peak quasi-static pressure produced by burning M10 propellant in closed and vented chambers. Combustion equations were written to define the heat generation and products of the burning propellant which act to increase the pressure in the shield. Temperature and pressure increases in the shield produced by burning the propellant are offset by radiation to the shield walls and gas flow from the shield through the vented panels. The equations describing these processes were coded into a computer program called GASSS which performed the calculations for M10 propellant burned in a Category V shield.

A. Combustion Equations

M10 propellant is 98% nitrocellulose with 13.15% nitration. Other major constituents are potassium sulfate and diphenylamine. Since nitrocellulose is the most active element in this propellant and since most of the propellant is nitrocellulose, the program assumes that M10 is all nitrocellulose. Thus, our calculations for energy produced from burning the propellant will be an upper limit. Based on 13.15% nitration of nitrocellulose and information in the literature on its products of combustion,[15] the reaction equations for burning nitrocellulose in the absence of air are:

73

$$C_6H_7(NO_2)_{2.63}O_5 \rightarrow 1.556\ CO_2 + 4.407\ CO + 1.001\ H_2 + 1.297\ N_2 + 2.622\ H_2O$$
$$+ 265.0\ \text{kilocalories} \tag{155}$$
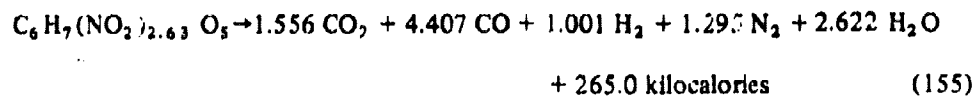
Secondary reactions involving the combustion of CO and H_2 in air are:

$$CO + 1/2O_2 \rightarrow CO_2 + 67.63\ \text{kilocalories} \tag{156}$$

and

$$H_2 + 1/2O_2 \rightarrow H_2O + 57.80\ \text{kilocalories} \tag{157}$$

The program was written so that during each time step, the products and energy of the reaction are calculated first without the presence of oxygen. Then, a calculation is performed to determine the amount of oxygen available. If there is sufficient oxygen present, the secondary reactions take place. When the oxygen in the chamber is depleted, only the primary reaction takes place. In vented and closed chambers, it is assumed that no oxygen enters from outside the structure due to positive pressure inside the chamber. The computer program also records the quantity of different gases present in the chamber at all times.

B. Gas Flow Equations

Determination of the pressure history for venting in a suppressive structure was accomplished by assuming quasi-steady, isentropic flow of a perfect gas. A check on the reliability of the perfect gas assumption was made by assuming complete combustion in an unvented chamber with no energy loss, and thermal equilibrium in the gases. Pressure was calculated using the ideal gas law and also using Van der Waal's equations for non-ideal gases, and the results were compared. For the pressures and molecular quantities involved, the ideal gas law was found to be quite accurate.

For the calculated pressure dissipation, the suppressive structure was idealized as two compartments separated by some vent area. If the ratio of atmospheric pressure to chamber pressure is less than

$$\left(\frac{2}{\gamma+1}\right)^{\left(\frac{1}{\gamma-1}\right)},$$

then supersonic flow equations are used. Otherwise, subsonic flow equations are utilized. The program causes the gas to vent proportionally to the quantity of each gas present.

If the flow is supersonic, the mass flow rate is determined by[16]

$$\frac{\Delta m_{1,t}}{\Delta t} = \frac{C_D A P_{1,t}}{\sqrt{R_{1,t}T_{1,t}/g}} \left[\sqrt{\frac{2\gamma}{\gamma+1}}\left(\frac{2}{\gamma+1}\right)^{1/(\gamma-1)}\right] \tag{158}$$

74

where

A = vent area of passage out of chamber

C_D = discharge coefficient of area A

P_1 = compartment pressure

R = universal gas constant

T = gas temperature

g = gravity constant

γ = ratio of specific heats

If the flow is subsonic, then

$$\frac{\Delta m_{1,t}}{\Delta t} = C_D A \left\{ \frac{2\gamma g}{(\gamma - 1)} \rho_{1,t} P_{1,t} \left[\left(\frac{P_{2,t}}{P_{1,t}} \right)^{2/\gamma} - \left(\frac{P_{2,t}}{P_{1,t}} \right)^{(\gamma+1)/\gamma} \right] \right\}^{1/2} \quad (159)$$

where

P_1 = density of gas in the chamber

P_2 = pressure outside the chamber

The rate of temperature change is given by

$$\dot{T}_{1,t} = T_{1,t}(\gamma - 1)\frac{\dot{m}_{1,t}}{m_{1,t}} \quad (160)$$

where

m = mass of the gas in the compartment, and the rate of pressure change is given by

$$\dot{P}_{1,t} = \frac{RT_{1,t}\dot{m}_{1,t}}{V_1} + \frac{P_{1,t}}{T_{1,t}} \dot{T}_{1,t} \quad (161)$$

where

V = volume of the compartment.

Pressure and temperature in the initial compartment at $t = t + \Delta t$ will then be

$$P_{1,t + \Delta t} = \dot{P}_{1,t}\Delta t + P_{1,t}$$
$$\quad (162)$$
$$T_{1,t + \Delta t} = \dot{T}_{1,t + \Delta t}\Delta t + T_{1,t}$$

Pressure and temperature outside the chamber were assumed to remain at ambient values.

C. Effects of Burning Rates and Radiant Heat Loss

Insufficient data were available to determine accurately the burning rates of piles of M10 propellant. A telephone conversation with Mr. William Seals,[17] of Picatinny Arsenal, produced the following results for M10:

<div align="center">

Burning Rate (in./sec)

Pressure (psi)	Single Perforation	Multi-perforation
5,000	1.49	1.38
9,000	2.24	2.07
11,000	2.58	2.18

</div>

These burning rates are obviously appropriate for interior gun ballistics, but are not appropriate for our purposes because the pressures in the suppressive structure for the worst case (no energy loss and instantaneous burning) are much smaller than the pressures in the table above. Measurements that Dr. Gary McKown[16] had taken when burning large quantities (500-1000 lb) of smoke mixes indicated burning rates of about 10 lb/sec. Measurements which he had taken while burning 10- and 50-lb quantities of magnesium and sodium nitrate illuminant produced burning rates varying from 4 to 100 lb/sec, depending on the quantity burned and the degree of confinement.

In view of this uncertainty in the burning rate, various rates were used in the calculations to show their influence on peak pressures in the Category V shield. Initially, burning rate was defined in units of lb/sec, and the pressure histories in the shield were computed using various quantities of propellant, several different burning rates, and various effective vent areas. The resulting pressures seemed to be unrealistically high, and this approach appeared to be inaccurate since the burning rate should depend on surface area and ambient pressure, and there should be radiant energy loss depending on the burning surface temperature and area. Thus, the computer program was modified to incorporate a linear burning rate and radiant heat loss. Because of the relatively low peak pressures, we neglected pressure dependency of the burning rate.

To convert a linear burning rate to a mass burning rate and burning surface area required that a burning geometry be assumed. Further, it was necessary that the burning surface be small initially and increase with burning time, which is characteristic of point ignition. The simplest geometry which could be assumed was a sphere with point ignition at the center. To permit radiation the sphere was treated as two hemispheres. For this geometry the effective increase in surface area with time is equal to that of a radially expanding sphere. The largest burning surface obtained in using this procedure is nearly identical to that of a cube of propellant of equal weight with one face unexposed; that is, on the floor. For example, equating volumes of the sphere and cube:

$$\frac{4}{3}\pi R^3 = \ell^3 \tag{163}$$

where R = radius of sphere (maximum)
ℓ = edge of cube

Solving Eq. (163) for R, one has

$$R = \left(\frac{3}{4\pi}\right)^{1/3} \ell \qquad (164)$$

The maximum surface area of the sphere is

$$4\pi r^2 = 4\pi \left(\frac{3}{4\pi}\right)^{2/3} \ell^2 \cong 4.84\ell^2 \qquad (165)$$

which is nearly the area of the five exposed sides of a cube of identical weight.

The above assumptions on bulk propellant burning and increase in burning surface were made to simplify a very complex burning process and provide for a representative increase in burning surface area and attendant increasing radiation losses after ignition. The use of a spherical geometry to describe the burning process offers the advantage of simplicity. It also allows for point ignition and growth in burning surface to a final value which is nearly the same in area as the exposed surfaces of a cube of equivalent weight. Thus, the simplified spherical geometry very nearly approximates the characteristics of the actual burning process.

The computer program was changed to incorporate a radial burning rate (units of in./sec) for the bulk propellant. By assuming negligible pressure dependency (relatively low peak pressures) and spherical geometries, burning rates of 10 lb/sec translates to 3.41 in./sec,* 7 lb/sec to 3.03 in./sec, and 4 lb/sec to 2.51 in./sec. The computer program was also modified to allow for radiant heat loss from the burning propellant and radiation loss from the gas in the chamber. Summaries of the output from these various techniques are contained in the tables that follow. The basic assumptions, in addition to the combustion and gas flow equations, are contained at the top of each table. We feel that the most accurate results are those which allow for radial burning rates (especially 3.40 in./sec) and at least some radiant energy loss. We estimate that the Category V shield has an effective vent area of 7.785 sq ft when vented. The effective vent area was determined by combining the vent areas of each component inside the side and roof panels by the equation

$$\frac{1}{\alpha_{eff}} = \frac{1}{\alpha_1} + \frac{1}{\alpha_2} + \ldots + \frac{1}{\alpha_n} \qquad (166)$$

where

α_{eff} = effective vent area

$\alpha_1, \alpha_2 \ldots \alpha_n$ = vent area of each component

---

*Time for burning various quantities (assuming spherical geometries) can be calculated from

$$T = \frac{\left(\dfrac{3}{4\pi} \dfrac{M}{0.0602 \text{ lb/in.}^3}\right)^{1/3}}{r}$$

where M is the mass of the propellant in pounds, and r is the burning rate in inches/second. For 3.41 in./sec burning rate, one can calculate that 10 lb burns in 1.00 second, 100 lb in 2.15 seconds, and 1000 lb in 4.64 seconds.

The side panel consists of

- a layer of angle irons with a vent area of 273 in.^{2},

- a layer of angle irons with a vent area of 485 in.^{2},

- three perforated plates with each plate having a vent area of 1410 in.^{2},

- four layers of aluminum mesh with each layer having a vent area of 3089 in.^{2}.

Thus, from Eq. (166), the effective vent area of a side panel is

$$\frac{1}{A_{V_{\text{side panel}}}} = \frac{1}{273} + \frac{1}{485} + \frac{1}{1410} + \frac{1}{3089}$$

$$A_{V_{\text{side panel}}} = 109 \text{ in.}^2$$

where $A_{V_{\text{side panel}}}$ is the effective vent area of a side panel.

The roof panel consists of

- a layer of angle irons with a vent area of 154 in.^{2},

- a layer of angle irons with a vent area of 273 in.^{2},

- three perforated plates with each plate having a vent area of 795 in.^{2},

- four layers of aluminum mesh with each layer having a vent area of 1742 in.^{2}.

Thus, from Eq. (166), the effective vent area of a roof panel is

$$\frac{1}{A_{V_{\text{roofpanel}}}} = \frac{1}{154} + \frac{1}{273} + \frac{3}{795} + \frac{4}{1742}$$

$$A_{V_{\text{roof panel}}} = 61.6 \text{ in.}^2$$

where $A_{V_{\text{roof panel}}}$ is the effective vent area of a roof panel.

Accounting for eight side panels and four roof panels, the total effective vent area of the Category V shield is

$$A_{V_T} = \frac{(8)(109.3) + (4)(61.63)}{144} = 7.785 \text{ ft}^2$$

Figure 12 was taken from the numerical results contained in Table XIV and contains plots of peak pressure versus vent area for a burning rate of 150 lb/sec, no radiation loss, and

78
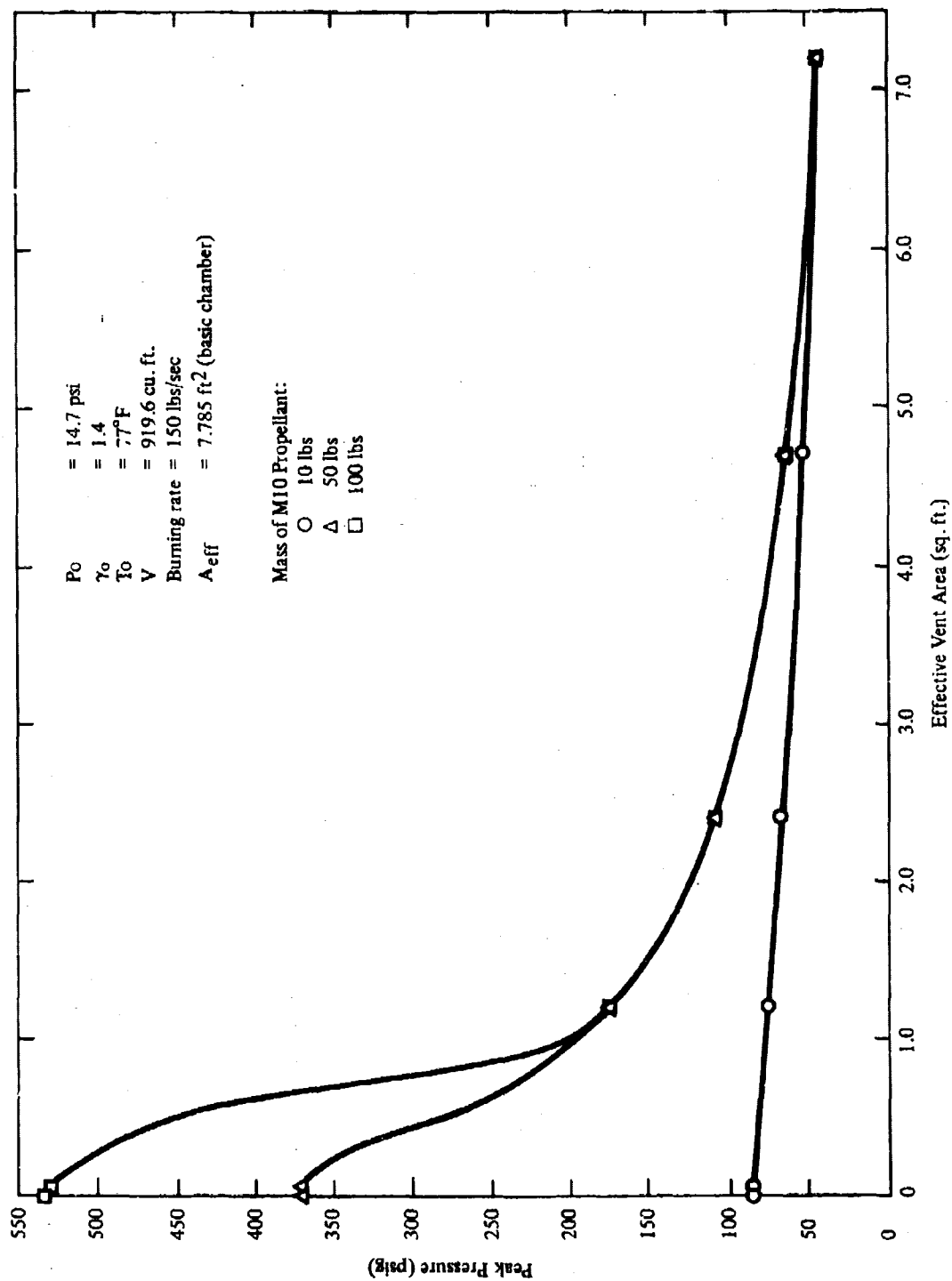
FIGURE 12 M10 PROPELLANT IN VENTED CHAMBER WITH NO RADIATION LOSS

79

TABLE XIV. M10 PROPELLANT IN VENTED CHAMBER WITH NO RADIATION LOSS

Assumptions:
Ambient Pressure	= 14.7 psi
Initial Ratio of Specific Heats	= 1.4
Ambient Temperature	= 77°F
Chamber Volume	= 919.6 cu ft
No radiation loss	
Constant mass/time burning rate	

Run No.	ΔT (sec)	Effective Vent Area (sq ft)	Burning Rate (lbs/sec)	Quantity (lbs)	Peak Pressure (psi)	Remarks
1	0.001	-0-	150	10	86	@ 0.067 sec
2	0.001	-0-	150	50	372	@ 0.100 sec
3	0.001	-0-	150	100	535	@ 0.334 sec
4	0.001	0.006	50	10	86	@ 0.200 sec
5	0.001	0.006	50	30	235	@ 0.600 sec
6	0.001	0.006	50	50	>368	max. not reached
7	0.001	0.006	50	100	>368	max. not reached
8	0.001	0.006	100	30	236	@ 0.300 sec
9	0.001	0.006	150	10	86	@ 0.067 sec
10	0.001	0.006	150	30	236	@ 0.200 sec
11	0.001	0.006	150	50	371	@ 0.334 sec
12	0.001	0.006	150	100	530	@ 0.667 sec
13	0.001	0.006	300	30	237	@ 0.100 sec
14	0.001	0.18	7	10	48	max. not reached
15	0.001	0.18	10	10	67	max. not reached
16	0.001	1.2	150	10	77	@ 0.067 sec
17	0.001	1.2	150	50	173	@ 0.255 sec
18	0.001	1.2	150	100	173	@ 0.255 sec
19	0.001	2.4	150	10	69	@ 0.067 sec
20	0.001	2.4	150	50	108	@ 0.203 sec
21	0.001	2.4	150	100	108	@ 0.203 sec
22	0.001	4.71	10	10	3	@ 0.120 sec
23	0.001	4.71	10	50	3	@ 0.120 sec
24	0.001	4.71	10	100	3	@ 0.120 sec
25	0.001	4.71	50	10	24	@ 0.136 sec
26	0.001	4.71	50	30	24	@ 0.136 sec
27	0.001	4.71	50	50	24	@ 0.136 sec
28	0.001	4.71	50	100	24	@ 0.136 sec
29	0.001	4.71	100	10	44	@ 0.100 sec
30	0.001	4.71	100	30	45	@ 0.121 sec
31	0.001	4.71	100	50	45	@ 0.121 sec
32	0.001	4.71	100	100	45	@ 0.121 sec
33	0.0005	4.71	124.4	10	51	@ 0.080 sec
34	0.001	4.71	124.4	10	51	@ 0.080 sec
35	0.005	4.71	124.4	10	49	@ 0.080 sec
36	0.01	4.71	124.4	10	46	@ 0.080 sec
37	0.001	4.71	124.4	50	54	@ 0.117 sec
38	0.001	4.71	124.4	100	54	@ 0.117 sec

Run No.	ΔT (sec)	Effective Vent Area (sq ft)	Burning Rate (lbs/sec)	Quantity (lbs)	Peak Pressure (psi)	Remarks
39	0.001	4.71	150	10	55	@ 0.066 sec
40	0.001	4.71	150	30	63	@ 0.113 sec
41	0.001	4.71	150	50	63	@ 0.113 sec
42	0.001	4.71	150	100	63	@ 0.113 sec
43	0.001	4.71	300	10	69	@ 0.033 sec
44	0.001	4.71	300	30	108	@ 0.100 sec
45	0.001	4.71	300	50	108	@ 0.103 sec
46	0.001	4.71	300	100	108	@ 0.103 sec
47	0.001	7.2	150	10	43	@ 0.066 sec
48	0.001	7.2	150	50	44	@ 0.079 sec
49	0.001	7.2	150	100	44	@ 0.079 sec

10-, 50-, and 100-lb quantities. Figure 13 was taken from the numerical results contained in Table XV and contains a plot of peak pressure versus vent area for a radial burning rate of 3.41 in./sec and radiation loss from the burning surface and surrounding gas. Figure 13 is for 10-lb quantities and probably predicts peak overpressure more accurately than Figure 12. Note that in the tables and figures, pressure is in units of psig; that is, pressure above atmospheric pressure.

TABLE XV. M10 PROPELLANT IN VENTED CHAMBER
WITH RADIATION LOSS

Assumptions: Ambient Pressure = 14.7 psi
Initial Ratio of Specific Heats = 1.4
Ambient Temperature ≈ 77°F
Chamber Volume = 919.6 cu ft
Radiation from produced gas and surrounding gas
Constant Radial Burning Rate

Run No.	ΔT (sec)	Effective Vent Area (sq ft)	Burning Rate (in./sec)	Quantity (lbs)	Peak Pressure (psi)	Remarks
1	0.005	0.18	3.41	10	60	@ 1.00 sec
2	0.01	0.18	3.03	10	57	@ 1.13 sec
3	0.01	0.18	2.51	10	53	@ 1.36 sec
4	0.01	0.3	3.41	10	55	@ 1.00 sec
5	0.01	0.6	3.41	10	43	@ 1.00 sec
6	0.01	0.6	2.51	10	33	@ 1.36 sec
7	0.01	1.2	3.41	10	25	@ 1.00 sec
8	0.01	1.2	2.51	10	16	@ 1.36 sec
9	0.01	2.0	3.41	10	12	@ 0.90 sec
10	0.01	4.0	3.41	10	2	@ 0.73 sec
11	0.01	4.71	3.41	10	1.4	@ 0.70 sec
12	0.01	4.71	3.41	50	1.4	@ 0.70 sec
13	0.01	4.71	3.41	100	1.4	@ 0.70 sec
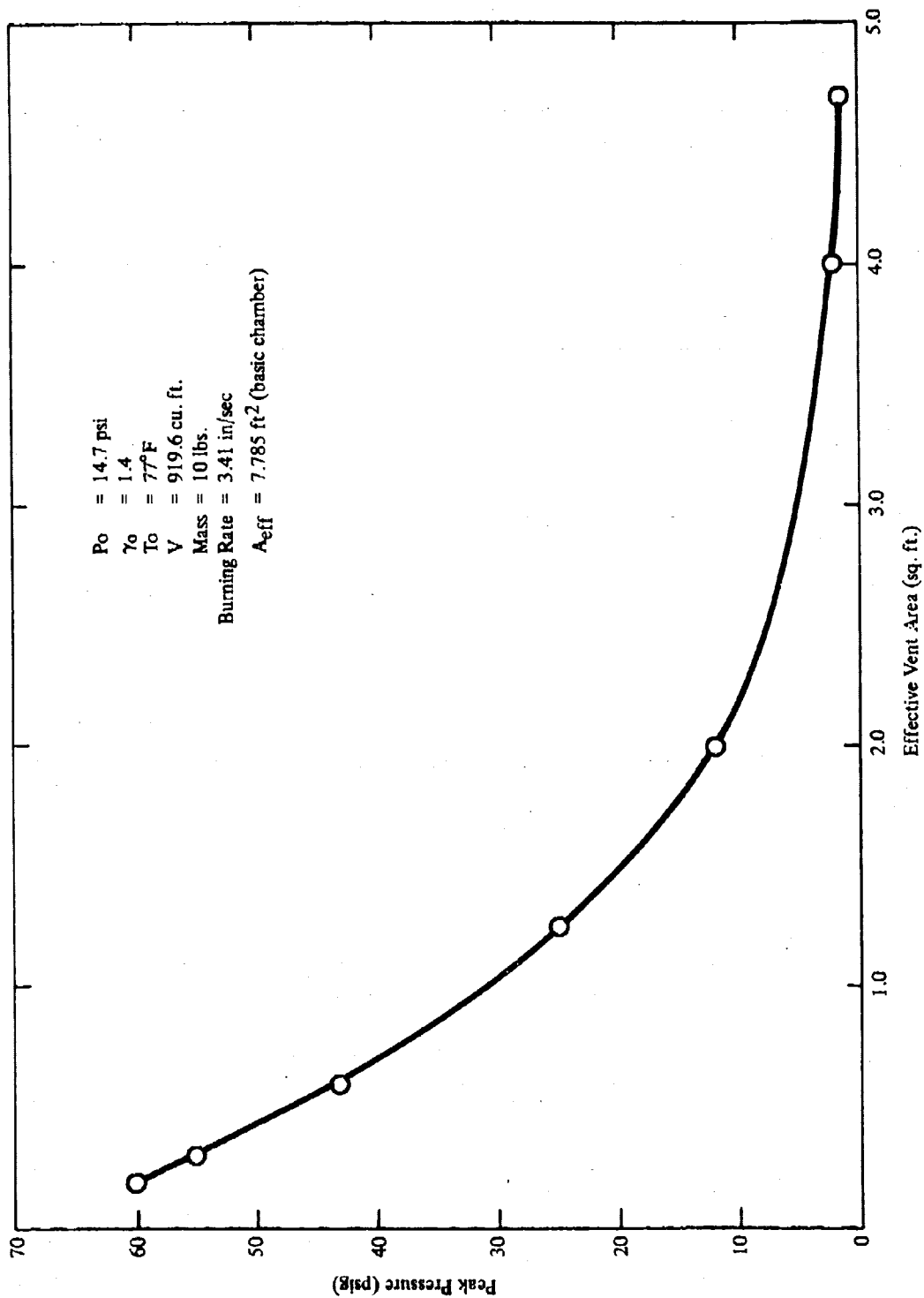
FIGURE 13. M10 PROPELLANT IN VENTED CHAMBER WITH RADIATION LOSS

P_o = 14.7 psi
γ_o = 1.4
T_o = 77°F
V = 919.6 cu. ft.
Mass = 10 lbs.
Burning Rate = 3.41 in/sec

A_{eff} = 7.785 ft² (basic chamber)

Effective Vent Area (sq. ft.)

Peak Pressure (psig)

D. Comparison with Experimental Results

Several tests have been conducted at NSTL where M10 propellant has been ignited inside a Category V suppressive structure. Although a written report has not yet been published Dr. Gary McKown of NSTL has revealed to us in a telephone conversation[18] that unconfined M10 propellant is a slow burner. During the Category V tests, 100-, 250-, and 600-lb quantities of M10 were burned inside the structure. The propellant was in cardboard boxes no more than a foot tall and was ignited from the top. The material burned like a "slow candle," with a burning time of approximately two or three seconds, depending on the weight of the propellant. It also appeared that the burning rate varied linearly with the mass of propellant.

During the tests there were large fireballs, no detonations, and very low quasi-static pressures inside the structure. From the films of the event, it appeared as if either the propellant or partially combusted products of the reaction had gotten outside the suppressive structure and ignited, thus contributing to the enormous fireball. Also, during the tests, all of the aluminum screening inside the structure and portions of other aluminum components were burned out or deteriorated, possibly due to the intense heat of the reaction. For one experiment, the top of the structure was covered with a piece of steel to control the vertical flow of the fireball. This steel roof had a hole burned through it by the end of the tests. The maximum pressure recorded during the tests was approximately 0.2 psig. Most of the time, however, pressure was so small that it was difficult to record.

As noted above, we suggested that Figure 13, with a radial burning rate of 3.41 in./sec which reduces to 100 lb burned in 2.15 seconds, 250 lb burned in 2.92 seconds, and 600 lb burned in 3.92 seconds, was the best figure to use to determine peak quasi-static pressure. From Table XV and Figure 13, for an effective vent area of 4.71 square feet and either 10, 50, or 100 lb of M10 propellant, one can see that the peak pressure is 1.4 psig. The initial Category V suppressive structure has an estimated effective vent area of 7.785 square feet. Since the interior aluminum baffles deteriorated after a few tests, the effective vent area increased 16.5% to 9.069 ft^2. This new effective vent area was determined by eliminating the last term in the equations used to calculate the effective vent areas of the side panels and roof panels. When one considers the effect of this additional vent area and the effect of energy losses due to burning of propellant outside the chamber, one would expect that the curve in Figure 13 is an upper limit conservative calculation. If these other terms, that is, additional vent area and radiant heat loss, were introduced into the computer program, lower and more accurate predictions would undoubtedly have been produced.

VI. DISCUSSION

Suppressive shielding was developed to house hazardous operations at explosives processing facilities. Should an accidental explosion occur, the shield is designed to contain or sharply reduce the blast overpressures, thermal effects, and fragment hazards produced. Nearby operations are thus shielded from the detrimental effects of the accident.

To properly design a shield to attenuate or completely contain the products of the explosion requires a knowledge of several complicated phenomena. These include:

83

1. overpressures inside and outside a vented enclosure produced by the detonation of high explosive charges or by the burning of propellants,

2. fragments generated by the accident,

3. thermal environment produced by the accident,

4. transient loading on the structural components of the shield produced by the overpressures, fragments, and thermal environment.

5. elastic-plastic response of the shield to the transient loading,

6. resistance of the shield to fragment penetration, and

7. attenuation of thermal effects by the shield.

Other aspects of the design include problems of entry and exit (for personnel, explosives, and utilities), cleanup, weatherproofing, lighting, air conditioning, and economy.

All of these problems have been addressed during the suppressive structures program, but not all of them have been satisfactorily resolved. Prediction of the thermal environment and its attenuation by the shield has received the least emphasis. Most other aspects of the design have been investigated in some detail, and procedures suitable for shield design have been developed; however, almost all aspects of the design can benefit from additional research.

The work documented in this report addresses principally items 1, 4, and 5. This work has included further developments in the application of energy methods for the analysis of structural response to blast loading, comparisons between predictions of structural response and test results, and predictions of pressure-time histories inside vented enclosures produced by burning propellant. The procedures developed for predicting pressures inside vented enclosures produced by a burning propellant are applicable to the design of Category V shields. Formulas and graphical solutions for structural analysis are applicable to the limit design of all shield groups.

Comparisons between analysis and experiment, which are described in this report and in earlier work[1,4,6] have shown that approximate energy methods provide good estimates for the elastic and elastic-plastic behavior of simple structural elements subjected to blast loading. This report contains a comprehensive summary of solutions developed during the suppressive structures program for the analysis of a large number of different structural elements. The comparisons also show that solutions for simple structural elements are not always suitable for the analysis of complex structures. Coupling, which can occur between structural components, can greatly attenuate the response of each component treated separately. However, even in this case we have shown that approximate energy solutions can give good results, but with some increase in complexity. Energy methods also lend themselves to graphical solutions which greatly simplify the complexity and labor involved in the solution process.

Although substantial progress has been made in the development of analytical procedures to support the design of suppressive shields additional work is needed in several areas. These include:

1. definition of the thermal environment produced by the detonation of a high explosive or by the burning of propellant,

2. methods to predict the thermal environment outside of a suppressive shield,

3. comparisons between measured and predicted pressures produced by burning propellants in vented enclosures,

4. failure criteria for dynamically loaded commercially available structural components. Commercially available components have been designed for optimum efficiency under static loading. A better understanding of their behavior when loaded by short duration high intensity loads is needed. This is particularly true for the failure of wide-flange beams in shear.

REFERENCES

1. W.E. Baker, P.S. Westine, P.A. Cox, and E.D. Esparza, "Analysis and Design of a Suppressive Structure for a Melt Loading Operation," Edgewood Arsenal Contract Report EM-CR-76056, Report No. 1, May 1976.

2. W.E. Baker and G.A. Oldham, "Estimates of Blowdown of Quasi-static Pressures in Vented Chambers," Edgewood Arsenal Contract Report EM-CR-76029, Report No. 2, Contract DAAA15-75-C-0083, SwRI, San Antonio, Texas, 1975.

3. E.D. Esparza, "Estimating External Blast Loads from Suppressive Structures," Edgewood Arsenal Contract Report EM-CR-76030, Report No. 3, Contract DAAA15-75-C-0083, SwRI, San Antonio, Texas, 1975.

4. P.S. Westine and P.A. Cox, "Additional Energy Solutions for Predicting Structural Deformations," Edgewood Arsenal Contract Report EM-CR-76031, Report No. 4, Contract DAAA15-75-C-0083, SwRI, San Antonio, Texas, 1975.

5. W.E. Baker and P.S. Westine, "Methods of Predicting Blast Loads Inside and Blast Loads Outside Suppressive Shields," Edgewood Arsenal Contract Report EM-CR-76026, Technical Report No. 5, November 1975.

6. P.S. Westine and W.E. Baker, "Energy Solutions for Predicting Deformations in Blast-Loaded Structures," Edgewood Arsenal Contractor Report EM-CR-76027, Report No. 6, November 1975.

7. P.A. Cox and E.D. Esparza, "Preliminary Design of a Suppressive Structure for a Melt Loading Operation," Edgewood Arsenal Contractor Report EM-CR-76028, Report No. 7, Contract DAAA15-75-C-0083, SwRI, San Antonio, Texas, 1975.

8. E.D. Esparza, W.E. Baker, and G.A. Oldham, "Blast Pressures Inside and Outside Suppressive Structures," Edgewood Arsenal Contract Report EM-CR-76042, Technical Report No. 8, December 1975.

9. W.E. Baker, P.A. Cox, E.D. Esparza, and P.S. Westine, "Design Study of a Suppressive Structure for a Melt Loading Operation," Edgewood Arsenal Contractor Report EM-CR-76043, Report No. 9, December 1975.

10. P.S. Westine, P.A. Cox, and E.D. Esparza, "Structural Analysis Emphasizing Energy Methods: Some Comparisons with Suppressive Shield Experiments," Minutes of the 17th Explosives Safety Seminar, Denver, Colorado, September 1976.

11. R.N. Schumacher and W.O. Ewing, Jr., "Blast Attenuation Outside Cubical Enclosures Made Up of Selected Suppressive Structure Panel Configurations," BRL Interim Memorandum Report No. 376, April 1975.

12. R.N. Schumacher, C.N. Kingery, and W.O. Ewing, Jr., "Airblast and Structural Response Testing of a 1/4-Scale Category I Suppressive Shield," BRL Memorandum Report No. 2623, May 1976.

13. W.E. Baker, *Explosions in Air*, University of Texas Press, Austin, 1973.

14. P.S. Symonds, "Survey of Methods for Plastic Deformation of Structures Under Dynamic Loading," Department of the Navy, Contract NONR 3248(01)(X). Naval Ship Research and Development Center, June 1967.

15. Jocelyn Field Thorpe and M.A. Whiteley, *Thorpe's Dictionary of Applied Chemistry*, Vol. IV, 4th edition, 1940, Longmans, Green & Co., London, pp. 506-516.

16. G.F. Kinney and R.G.S. Sewell, "Venting of Explosions," NWC Technical Memorandum 2448, Naval Weapons Center, China Lake, California, July 1974.

17. Telephone conversation with Mr. William Scals of Picatinny Arsenal.

18. Telephone conversation with Dr. Gary McKown, Edgewood Arsenal at the National Space Test Laboratory (NSTL) in Bay St. Louis, Mississippi.

19. D.A. Martin and G.L. McKown, "Proof Testing of a Candidate Category III Suppressive Shield," Edgewood Arsenal Tech. Report No. EM-TR-76064, August 1976.

DISTRIBUTION OF SUPPRESSIVE SHIELDING REPORTS

Addressee	No. of Copies
Commander Rocket Propulsion Laboratory Attn: Mr. M. Raleigh Edwards Air Force Base, CA 93523	1
Commander HQ, Armament Development Test Center Attn: DOM/Mr. S. Reither Eglin Air Force Base, FL 32542	1
Commander Hill Air Force Base Attn: MMNTR/Mr. Cummings Clearfield, UT 84406	1
Commander Norton Air Force Base Attn: AFISC-SEV/Mr. K. Collinsworth San Bernardino, CA 92409	1
Commander Air Force Civil Engineering Center Attn: AFCEC-DE/LTC Walkup Tyndall Air Force Base Panama City, FL 32401	1
Commander HQ Air Force Logistics Command Attn: MMWM/CPT D. Rideout IGYE/Mr. K. Shopher Wright-Patterson Air Force Base Dayton, OH 45433	1 ea
Commander Naval Ordnance Systems Command Attn: Code ORD 43B/Mr. A. Fernandes Washington, DC 20360	1
Commander Explosives Safety Attn: ADTC/SEV (Mr. Ron Allen) Eglin Air Force Base, FL 32542	1

Commander   1
Bureau of Naval Weapons
Attn: Code F121/Mr. H. Roylance
Department of the Navy
Washington, DC 20360

Commander   1
Naval Ship Research & Development Center
Attn: Code 1747/Mr. A. Wilner
Bethesda, MD 20034

Commander   1
Naval Explosive Ordnance Disposal Facility
Attn: Code 501/Mr. L. Wolfson
Indianhead, MD 20640

Commander   1
Naval Ordnance Systems Command
NAPEC
Naval Ammunition Depot
Attn: ORD-04M/B/X-5/Mr. L. Lecnard
Crane, IN 47522

Commander   1
US Naval Surface Weapons Center
Attn: Mr. J. Proctor
Whiteoak, MD 20904

Chairman   5
DOD Explosives Safety Board
Attn: COL P. Kelly, Jr.
Forrestal Building GB-270
Washington, DC 20314

Joint Army-Navy-Air Force Conventional   5
Ammunition Production Coordinating Group
USA Armament Command
Attn: Mr. Edward Jordan
Rock Island, IL 61201

HQDA (DAEN-MCC-I/Mr. L. Foley)   1
Washington, DC 20314

HQDA (DAEN-MCE-D/Mr. R. Wight)   1
Washington, DC 20314

Director   1
USAMC Field Safety Activity
Attn: AMXOS-TA/Mr. Olson
Charlestown, IN 47111

Commander   1 ea
US Army Materiel Command
Attn: AMCCG
       AMCRD/Dr. Kaufman
       AMCSF/Mr. W. Queen
       AMCPM-CS/COL Morris
5001 Eisenhower Ave.
Alexandria, VA 22333

Office of the Project Manager for   3
Munition Production Base Modernization
   and Expansion
Attn: AMCPM-PBM-E/Mr. Dybacki
USA Materiel Command
Dover, NJ 07801

Commander   1 ea
US Army Armament Command
Attn: AMSAR-EN/Mr. Ambrosini
       AMSAR-SC/Dr. C. Hudson
       AMSAR-SF/Mr. J. Varcho
       AMSAR-TM/Mr. Serlin, Mr. T. Fetter, Mr. S. Porter
       AMSAR-MT/Mr. A. Madsen, Mr. G. Cowan, CPT Burnsteel
Rock Island Arsenal
Rock Island, IL 61201

Commander   1 ea
USAMC Ammunition Center
Attn: Mr. J. Byrd
       AMXAC-DEM/Mr. Huddleston
                 Mr. Sumpterer
Savanna, IL 61074

Commander   1 ea
Frankford Arsenal
Attn: Mr. F. Fidel, Mr. E. Rempler
Bridge and Tacony Sts.
Philadelphia, PA 19137

Commander
Picatinny Arsenal
Attn: Mr. Saffian   3
       Mr. J. Cannovan   1 ea
       Mr. Hickerson
       Mr. I. Forsten
Dover, NJ 07801

Commander   1
USA Test and Evaluation Command
Attn: AMSTE-NB
Aberdeen Proving Ground, MD 21005

Commander   1 ea
Dugway Proving Ground
Attn: Dr. Rothenburg
       Mr. P. Miller
Dugway, UT 84022

Commander   1
Cornhusker Army Ammunition Plant
Grand Island, NE 68801

Commander   1
Indiana Army Ammunition Plant
Charleston, IN 47111

Commander   1
Iowa Army Ammunition Plant
Burlington, IA 52502

Commander   1
Joliet Army Ammunition Plant
Joliet, IL 60436

Commander   1
Kansas Army Ammunition Plant
Parsons, KS 67357

Commander   1
Longhorn Army Ammunition Plant
Marshall, TX 75671

Commander   1
Lone Star Army Ammunition Plant
Texarkana, TX 75502

Commander   1
Louisiana Army Ammunition Plant
Shreveport, LA 71102

Commander   1
Milan Army Ammunition Plant
Milan, TN 38358

Commander   1
Radford Army Ammunition Plant
Radford, VA 24141

Commander   1
Sunflower Army Ammunition Plant
Lawrence, KS 66044

Commander   1
Lake City Army Ammunition Plant
Attn: Mr. John Jacobi
Independence, MO 64056

Commander   1
Ravenna Army Ammunition Plant
Ravenna, OH 44266

Commander   1
Pine Bluff Arsenal
Pine Bluff, AR 71601

Director   3
US Army Materiel Systems Analysis Activity
Aberdeen Proving Ground, MD 21005

Director   5
US Army Ballistics Research Laboratories
Attn: Mr. R. Vitali
Aberdeen Proving Ground, MD 21005

Division Engineer   1 ea
US Army Engineer Division, Huntsville
Attn: HNDED-R/Mr. Dembo
            Mr. W. Char
P.O. Box 1600, West Station
Huntsville, AL 35807

US Army Engineer Division   1
Waterways Experimental Station
P.O. Box 631
Vicksburg, MS 39180

Director   1
USAMC Intern Training Center
Attn: Dr. G. Chiang
Red River Depot
Texarkana, TX 75502

Dr. Robert D. Siewert   1
NASA Lewis Laboratory
21000 Brook Park Rd
Cleveland, OH 44135

Mr. George Pinkas   1
Code 21-4
NASA Lewis Laboratory
21000 Brook Park Rd
Cleveland, OH 44135

Mr. W. H. Jackson   1
Deputy Manager for Engineering
Atomic Energy Commission
P.O. Box E
Oak Ridge, TN 37830

Mr. Erskine Harton   1
US Department of Transportation
Washington, DC 20315

Dr. Jean Foster   1
US Department of Transportation
Washington, DC 20315

Mr. Frank Neff   1
Mound Laboratory
Monsanto Research Corp.
Miamisburg, OH 45342

Ms. Trudy Prugh   1
Mound Laboratory
Monsanto Research Corp.
Miamisburg, OH 45342

Commander   1
Naval Weapons Laboratory
Attn: Mr. F. Sanches
Dahlgren, VA 22448

Dr. W. E. Baker   1
Southwest Research Institute
San Antonio, TX 78284

Division Engineer   1
US Army Engineer Division, Fort Belvoir
Fort Belvoir, VA 22060

Commander   1
Naval Sea Systems Command
Washington, DC 20315

Mr. Billings Brown   1
Hercules, Inc.
Box 98
Magna, UT 84044

Mr. John Komos   1
Defense Supply Agency
Cameron Station
Alexandria, VA 22030

Office of the Project Manager for Chemical   2
  Demilitarization and Installation Restoration
Edgewood Arsenal
Aberdeen Proving Ground, MD 21010

Edgewood Arsenal
Technical Director
Attn: SAREA-TD-E   1
Foreign Intelligence Officer   1
Chief, Legal Office   1
Chief, Safety Office   1
CDR, US Army Technical Escort Center   1
Author's Copy, Manufacturing Technology Directorate   3
Aberdeen Proving Ground, MD 21010

Edgewood Arsenal
Director of Biomedical Laboratory
Attn: SAREA-BL-M   1
       SAREA-BL-B   1
       SAREA-BL-E   1
       SAREA-BL-H   1
       SAREA-BL-R   1
       SAREA-BL-T   1
Aberdeen Proving Ground, MD 21010

Edgewood Arsenal
Director of Chemical Laboratory
Attn: SAREA-CL-C   1
       SAREA-CL-P
Aberdeen Proving Ground, MD 21010

Edgewood Arsenal
Director of Development & Engineering
Attn: SAREA-DE-S   4
Aberdeen Proving Ground, MD 21010

Edgewood Arsenal
Director of Manufacturing Technology
Attn: SAREA-MT-TS   2
        SAREA-MT-M   1
Aberdeen Proving Ground, MD 21010

Edgewood Arsenal
Director of Product Assurance
Attn: SAREA-PA-A   1
        SAREA-PA-P   1
        SAREA-PA-Q   1
Aberdeen Proving Ground, MD 21010

Edgewood Arsenal
Director of Technical Support
Attn: SAREA-TS-R   2
        SAREA-TS-L   3
        SAREA-TS-E   1
Aberdeen Proving Ground, MD 21010

Aberdeen Proving Ground   1
Record Copy
CDR, APG
Attn: STEAP-AD-R/RHA
APG-Edgewood Area, BLDG E5179
Aberdeen Proving Ground, MD 21005

Aberdeen Proving Ground   1
CDR, APG
Attn: STEAP-TL
APG, Aberdeen Area
Aberdeen Proving Ground, MD 21005

DEPARTMENT OF DEFENSE
Administrator   12
Defense Documentation Center
Attn: Accessions Division
Cameron Station
Alexandria, VA 22314

Commander
Edgewood Arsenal   1
Attn: SAREA-DM
Aberdeen Proving Ground, MD 21010